Quantifying the impact of non-pharmaceutical interventions on COVID-19 in Canada

Zihuai Shi

Department of Mathematics and Statistics

McGill University, Montréal

July, 2022

A thesis submitted to McGill University in partial fulfillment of the requirements of the degree of

Master of Science

Abstract

This research is concerned with measuring the effect of various non-pharmaceutical interventions (NPI), including the policies of the Government of Québec (Canada), in the fight against the severe acute respiratory syndrome coronavirus 2 (SARS-CoV-2), which causes the disease known as COVID-19. The effect of such interventions can be measured through the effective reproduction rate R_t, a fundamental epidemiological factor representing the average number of infections generated at time t by any infected and contagious individual. A prominent method for computing R_t, the `Estimate_R` algorithm developed by Cori et al. (2013), is investigated. As the algorithm is deterministic, the confidence interval it produces does not have a probabilistic interpretation. A Monte Carlo approach is used to circumvent this problem. Two strategies are developed, based either on Poisson regression or on a state-space model. Evidence was found to the effect that (i) there is an association between two NPIs (school closure and curfew) and reduced R_t; and (ii) a curfew tends to slow down the change in transmission rate when the controlled variable (school closure) is held constant.

Résumé

Ce travail porte sur la quantification de l'effet de diverses interventions non pharmaceutiques (INP), dont les politiques mises en place par le Gouvernement du Québec (Canada), dans la lutte au coronavirus (SARS-CoV-2) responsable de la maladie appelée COVID-19. L'effet de telles interventions peut être mesuré à travers le taux de reproduction effectif R_t, facteur épidémiologique déterminant qui renseigne quant au nombre moyen d'infections générées au temps t par un individu infecté et contagieux. La méthode `Estimate_R` proposée par Cori et coll. (2013) pour le calcul du coefficient R_t est étudiée. Sachant qu'elle s'appuie sur un algorithme déterministe, l'intervalle de confiance auquel elle conduit n'a pas d'interprétation probabiliste. On propose une approche de type Monte-Carlo pour remédier à ce problème. Deux stratégies sont élaborées, l'une fondée sur une régression de Poisson et l'autre sur un modèle espace-état. Il appert que (i) deux INP (fermetures d'écoles et couvre-feu) sont liées à une réduction du coefficient R_t ; (ii) un couvre-feu contribue au ralentissement de la variation du taux de transmission une fois pris en compte l'effet des fermetures d'établissements scolaires.

Acknowledgements

I would like to thank first and foremost my supervisors Professors David Stephens and Christian Genest for their guidance and commitment throughout my Master's studies, and for their confidence in my work.

Moreover, I would like to thank the Department of Mathematics and Statistics at McGill University, the Natural Sciences and Engineering Research Council, the Canada Research Chair in Dependence Modelling, and the Trottier Institute for Science and Pubic Policy for financial support that made the completion of this project possible.

I would also like to thank my colleagues and friends: Professor Courtney Paquette for her insights on parameter optimization; Haoyu Wu for her assistance in understanding key concepts; Magid Sabbagh for his guidance and support in understanding key concepts and in navigating the **R** software; Louis Arsenault-Mahjoubi for his support in understanding key concepts; and Victor Dumitru for offering valuable advice to improve the writing of this thesis.

Finally, I would like to express my gratitude to my parents, Shucai Shi and Shulan Zhao, for their everlasting support and faith in me.

Table of Contents

List of Figures

List of Tables

Chapter 1

Introduction

1.1 Background

Towards the end of 2019, a novel virus emerged in the city of Wuhan (Hebei province, China) causing severe pneumonia. On 11 February 2020, the causative agent was named "severe acute respiratory syndrome coronavirus 2" (SARS-CoV-2) by the World Health Organization (WHO), and the disease it causes was called COVID-19. On 20 March 2020, WHO declared it a worldwide pandemic, as it very quickly spread to other countries around the world. From January 2020 to January 2022, more than 3.25 million cases were confirmed in Canada, with deaths exceeding 36,000 persons.

In 2020, non-pharmaceutical interventions (NPIs) were the only option to moderate the spread of the virus. No vaccines were yet available. Confronted with the worldwide COVID-19 pandemic under rapidly changing epidemiological situations, most governments implemented highly restrictive and intrusive interventions, including stay-at-home orders and the closure of all non-essential businesses.

In Canada, the year 2021 was characterized by severe financial stress for businesses due to lockdowns and public resistance to pandemic guidelines. Federal and provincial governments instigated policies to mitigate the propagation of the disease. However, were they effective? Acquiring knowledge on the effectiveness of NPIs to mitigate the

spread of the virus is critical for stakeholders to implement interventions and combat a resurgence of COVID-19 or any other future disease outbreak.

1.2 Rationale

A key building block to analyzing the effectiveness of NPIs is to quantify their impact. A good measure of the impact of NPIs is the effective reproduction number, R_t. It is a key epidemic parameter that estimates the average number of secondary cases of disease caused by a single infected individual at time t over their infectious period.

This thesis is aimed at developing a statistically rigorous approach to estimating R_t and constructing an associated confidence interval, as well as investigating the impact of NPIs, in particular, the effect of the curfew that was imposed in Québec, Canada over the period from 9 January to 28 May 2021.

A critical look is first cast on the most popular way of estimating R_t, the `estimate_R` algorithm developed by Cori et al. [7]. It is observed that confidence intervals cannot be derived from this algorithm, considering that the model is deterministic. The most serious ramification of the lack of a confidence interval is that it is then impossible to assess the nature of changes in R_t, leading to biased conclusions drawn from such analyses.

This thesis employs a synthetic R_t example to emphasize the need for an accurate confidence interval in reaching credible results. It further proposes a Monte Carlo simulation strategy to construct a confidence interval for R_t and presents two methods for generating samples, performing forward-simulation with a Poisson distribution and emulating samples using a state-space model.

Chapter 2

Literature and Data

2.1 Related Works

The existing literature on the impact of NPIs on the spread of COVID-19 is rich. The study published by the Imperial College COVID-19 Response Team [8] focused on NPI's impact on reducing mortality. The study of Flaxman et al. [9] used the effective reproduction number, R_t, to quantify the impact of NPIs in Sweden. The study of Haug et al. [13] quantified the impact on R_t of 6,068 hierarchically coded NPIs implemented in 79 territories. The study of Brauner et al. [3] estimated the effectiveness of NPIs with a Bayesian hierarchical model, and revealed that, by implementing effective interventions, certain countries could control the in-country epidemic while avoiding stay-at-home orders.

This thesis will focus on two comparable studies. The Institut national de santé publique du Québec (INSPQ) [16] used a method developed by Cori et al. [7] to quantify R_t. The study of Liu et al. [15] employed panel (longitudinal) regression to quantify the effectiveness of 13 categories of NPIs in reducing SARS-CoV-2 transmission, and uncovered evidence for an association between two NPIs (school closure and internal movement restrictions) and reduced R_t.

2.2 Reproduction Number

The effective reproduction number, R_t, is a useful indicator of the impact of NPIs. To understand R_t, we need to formulate an epidemic model. The model we use is a type of compartmental model called the SEIR model. Compartmental models can describe the spread of a disease within a population.

The SEIR model describes the flow of individuals through four mutually exclusive stages of infection: susceptible, exposed, infected, and recovered. This model can be used to compute the infected population and the number of deaths of this epidemic. Four compartments, viz. Susceptible $S(t)$, Exposure $E(t)$, Infectious $I(t)$, and Recovered $R(t)$, were used to denote the number of individuals in the four groups as functions of time t.

The COVID-19 dynamics are modelled by a system of four differential equations, viz.

$$\begin{aligned}
\frac{dS}{dt} &= N - \underbrace{\beta I S \frac{1}{N}}_{\text{infection}} + \underbrace{\omega R}_{\text{lost immunity}}, \\
\frac{dE}{dt} &= \underbrace{\beta I S \frac{1}{N}}_{\text{infection}} - \underbrace{\sigma E}_{\text{latency}}, \\
\frac{dI}{dt} &= \underbrace{\sigma E}_{\text{latency}} - \underbrace{\gamma I}_{\text{recovery}} - \underbrace{(\mu + \alpha) I}_{\text{death}}, \\
\frac{dR}{dt} &= \underbrace{\gamma I}_{\text{recovery}} - \underbrace{\omega R}_{\text{lost immunity}} - \underbrace{\mu R}_{\text{death}}.
\end{aligned}$$

Table 2.1 summarizes the parameters used in the model. Bjørnstad [2] showed that the transmission rate can be calculated using the product $\{\sigma/(\sigma+\mu)\} \times \{\beta/(\gamma+\mu+\alpha)\}$. The basic reproductive number measures transmission by a specific group of individuals with the same date of infection or symptom onset; such a group is often referred to as a cohort of individuals. The instantaneous reproductive number R_t measures transmission at a specific point in time; it is more appropriate for analyses estimating the reproductive number of the infected population on specific dates [11].

Table 2.1: List of parameters used in the SEIR model

Name	Description
β	Infectivity
ω	Lost immunity rate
σ	Latency
α	Death due to infection rate
γ	Recovery rate
μ	Death rate
N	Total population

As this thesis is aimed at investigating how NPIs have affected transmission at a given point in time, it is of interest to estimate R_t.

Figure 2.1 presents a visualization of the SEIR model generated by `Anylogic` at a random time t. Here, the number under each compartment means the current number of people in that compartment. One advantage of this model is that it is dynamic, meaning that it captures the changes on each day.

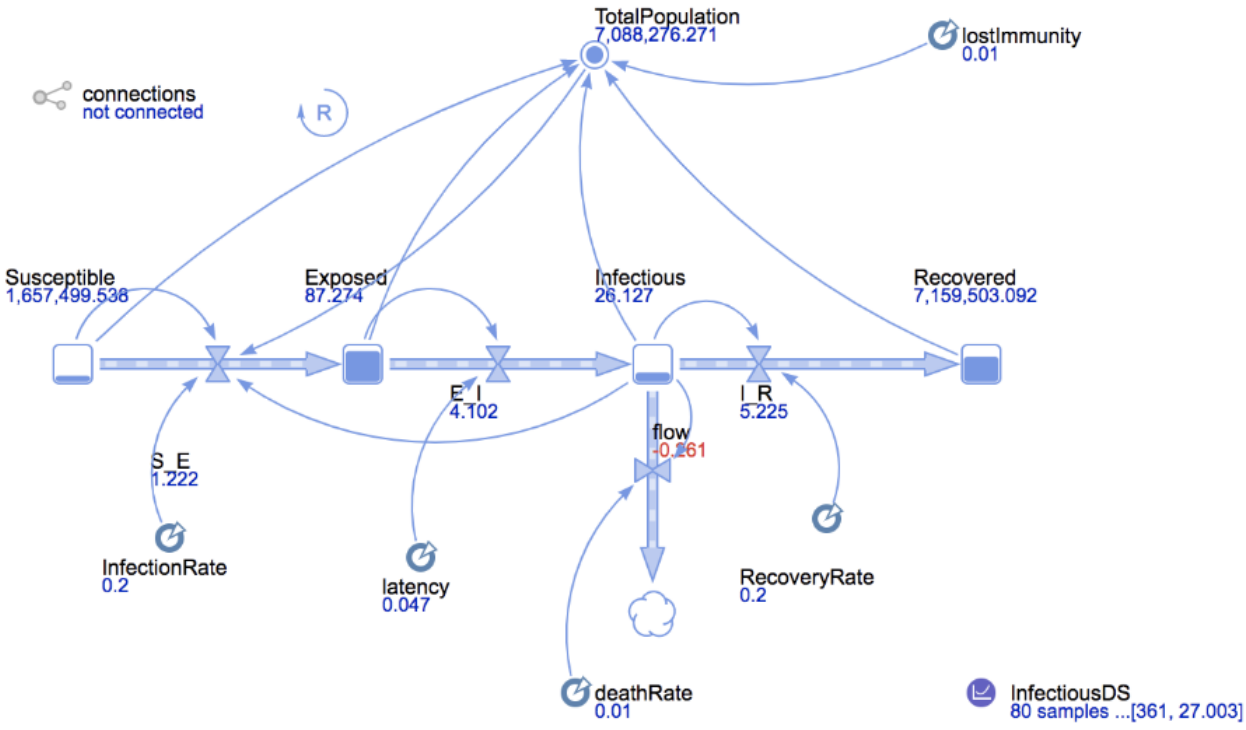

Figure 2.1: Visualization of SEIR model

Researchers proposed various ways of estimating R_t for COVID-19. The most prominent is the study of Cao et al. [5], which is one of the earliest studies. These authors derived an equation to compute R_t for COVID-19 following a similar methodology to that used by Lipsitch et al. [14] to estimate R_t for the 2003–04 SARS disease outbreak.

Instead of deriving the equation and constructing the algorithm, one can use existing algorithms to estimate R_t. A prominent algorithm to compute R_t is the `estimate_R` function in the `EpiEstim` package developed by Cori et al. [7]. In Canada, for example, the Institut national de santé publique du Québec (INSPQ) [16] used the `estimate_R` function to compute R_t. Nouvellet et al. [18] also used the `EpiEstim` function to calculate the effective reproduction number at the time of infection to parameterize the relationship between transmission and mobility.

2.3 Monte Carlo Method

Dennis et al. [20] gave the following definition of the notion of a confidence interval:

> "An interval estimator is a rule specifying the method for using the sample measurements to calculate two numbers that form the endpoints of the interval. Interval estimators are commonly called confidence intervals. The upper and lower endpoints of a confidence interval are called the upper and lower confidence limits, respectively. The probability that a (random) confidence interval will enclose θ (a fixed quantity) is called the confidence coefficient. From a practical point of view, the confidence coefficient identifies the fraction of the time, in repeated sampling, that the intervals constructed will contain the target parameter θ. If we know that the confidence coefficient associated with our estimator is high, we can be highly confident that any confidence interval, constructed by using the results from a single sample, will enclose θ."

In short, a confidence interval measures the degree of uncertainty associated to a sampling method, and its width is a measure of the accuracy of an estimate. Obtaining appropriate confidence intervals is critical to analyzing data and drawing conclusions.

The popular `estimate_R` algorithm has a critical limitation: because the model is deterministic, no confidence interval is associated with it. This thesis proposes a solution based on Monte Carlo simulations to construct confidence intervals.

2.4 State-Space Model

State-space models are a type of auto-regressive time series model that enables us to account for uncertainty in the observation model. They are widely used and go by a variety of names, including structural models (econometrics), dynamic linear models (statistics), Bayesian forecasting models (statistics), linear system models (engineering), and Kalman filtering models (control engineering).

A state-space model is consistent with an observation component and a state component. Here, the stochastic state components are associated with estimation errors. These stochastic errors have unique variances, allowing the confidence intervals to be constructed around each of the state components.

The state-space model's primary advantage lies in its ability to create and estimate custom models. This thesis employs state-space models to emulate samples and uses the Monte Carlo method to obtain confidence intervals.

2.5 Data Collection

The three main sources of data used for this analysis are the COVID-19 Canada Open Data Working Group [1], the Institut national de santé publique du Québec (INSPQ) [16], and the Canadian Institute of Health Informatics (CIHI) [4]. R Studio software Version 1.2.5001 was used to process the data and generate figures. The majority of the figures in

this thesis cover data from 1 April 2020 to 1 December 2021, except for a few figures in Chapter 3 that focus on specific times of NPI deployments.

For the period of interest, the total population of Québec is estimated at 8,604,500 people, whereas Ontario has a population of 14,789,778 people. The figure for Québec is drawn from the 2020 edition of the Bilan démographique du Québec [16] published by INSPQ. The figure for Ontario is drawn from [19], which used the 2020 population estimates from Statistics Canada (released in February 2021 and based on the 2016 Census).

The COVID-19 Canada Open Data Working Group collects publicly available information on confirmed and presumptive positive cases during the ongoing COVID-19 outbreak in Canada. All data were collected from publicly available sources, including government reports and news media.

INSPQ is an expertise and reference centre that contributes to the understanding and decision-making on issues of public health. In this thesis, the cases and R_t data provided by INSPQ are used for comparison purposes.

The Canadian Institute of Health Informatics (CIHI) maintains a comprehensive scan of federal and provincial government interventions related to COVID-19, sourced from government releases and websites, national indigenous organizations, as well as regulatory bodies for health professionals. CIHI provides data on a wide range of interventions, including vaccines, health workforce capacity, travel restrictions, and public information. This thesis is focused on non-pharmaceutical interventions (NPIs) relating to openings and closures, and physical distancing, viz.

(i) closures of elementary and secondary schools;

(ii) closures of public spaces (e.g., places of worship, parks, museums);

(iii) closures of non-essential businesses (e.g., restaurants, bars, karaoke lounges);

(iv) restrictions on indoor and outdoor gatherings;

(v) implementation of curfews.

2.5.1 Reported Cases

The data used in this thesis consist of daily case counts, daily tests, and cumulative tests of COVID-19 for Canada and its 10 provinces, retrieved from the Canada Open Data group.

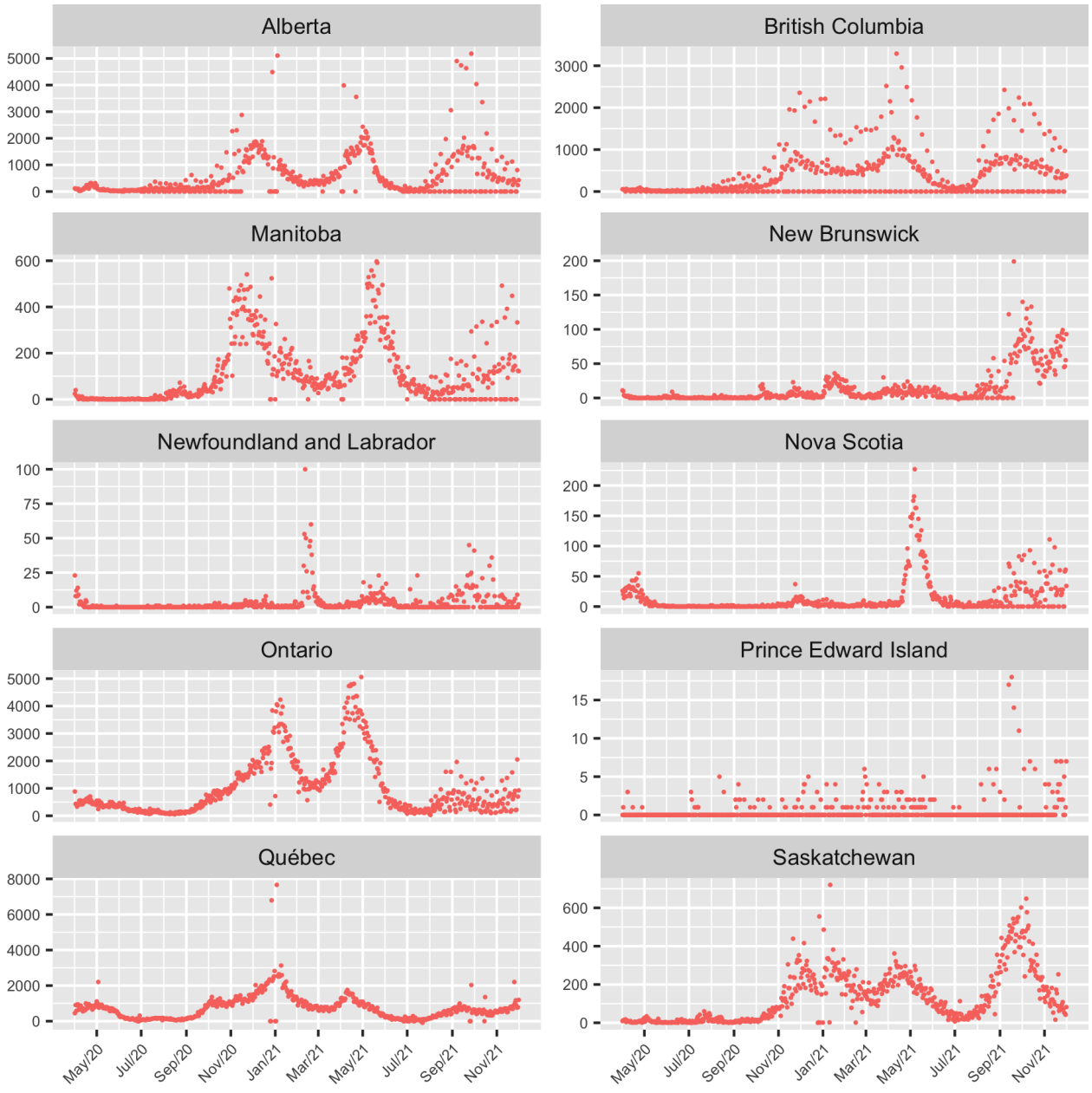

Figure 2.2: Daily reported incidence in the 10 provinces of Canada over the period from 1 April 2020 to 1 December 2022

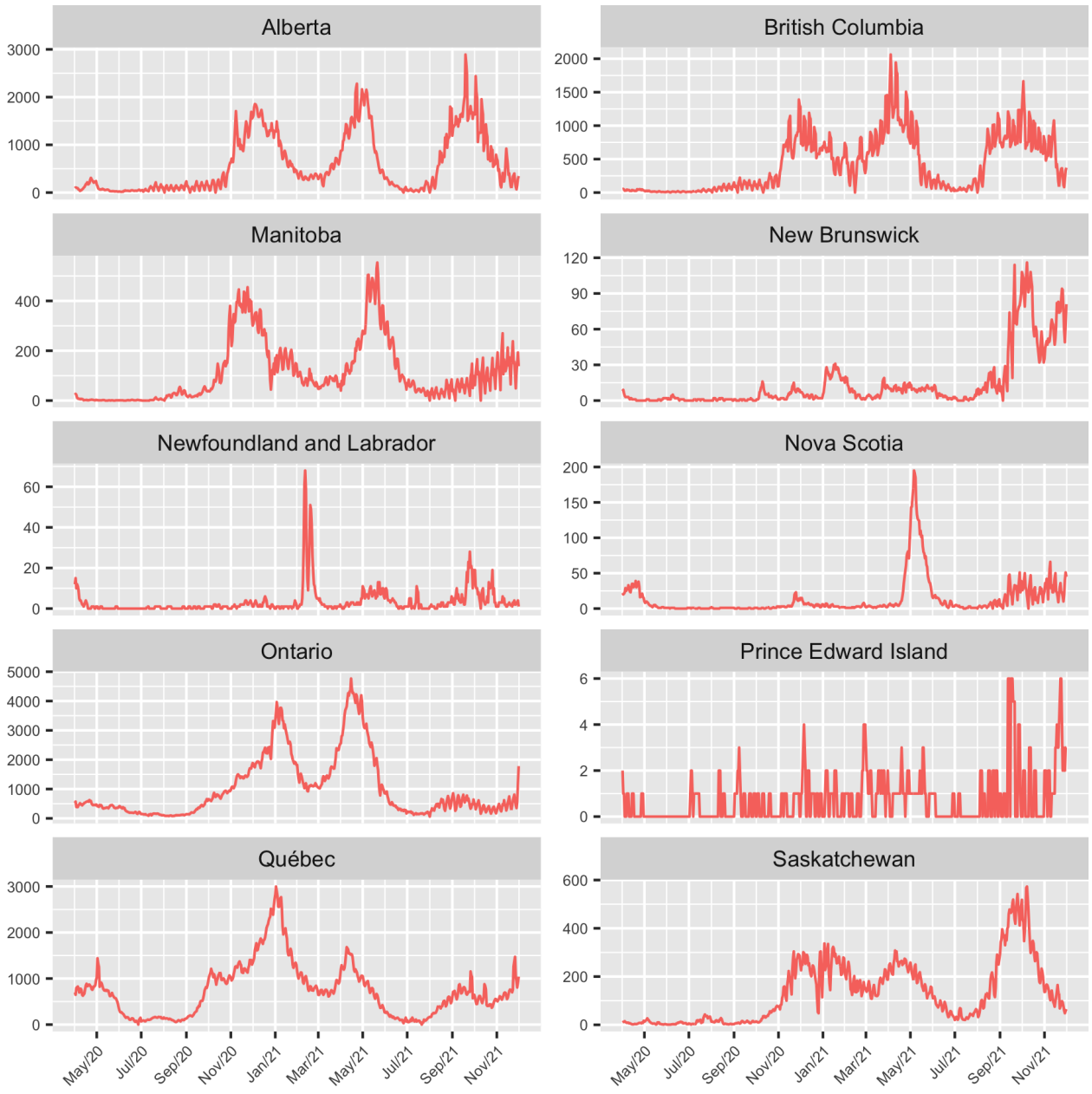

Figure 2.3: Adjusted daily reported incidence in the 10 provinces of Canada over the period from 1 April 2020 to 1 December 2022

In Figure 2.2, some outliers occur not because there is an unusually large number of cases on any given day. These outliers occur because the authorities periodically realized that they had missed some cases and added them all in one day. To achieve more accurate results, the actual count of data must be used instead of the reported count, i.e., the data after fixing the initial data entry errors.

Figure 2.3 shows the daily reported incidence in the 10 provinces of Canada with slight adjustments over the period from 1 April 2020 to 1 December 2022. Some administrative errors were corrected. The reported incidences for Québec on the 24th, 25th, 26th, and 27th of December 2020 were 2349, 0, 0, 6793, respectively. The values for the 27th were redistributed in part to the 25th and 26th.

2.5.2 Intervention Data

Data related to government interventions were acquired from Health Canada, CIHI [4]. The government developed a regional level colour coding to indicate relative level of rate of transmission. The highest risk level was designated red. In Figure 2.4, the colored dots signify the imposing or easing of interventions. Section A.1 in the Appendix contains an identical plot with shaped dots instead.

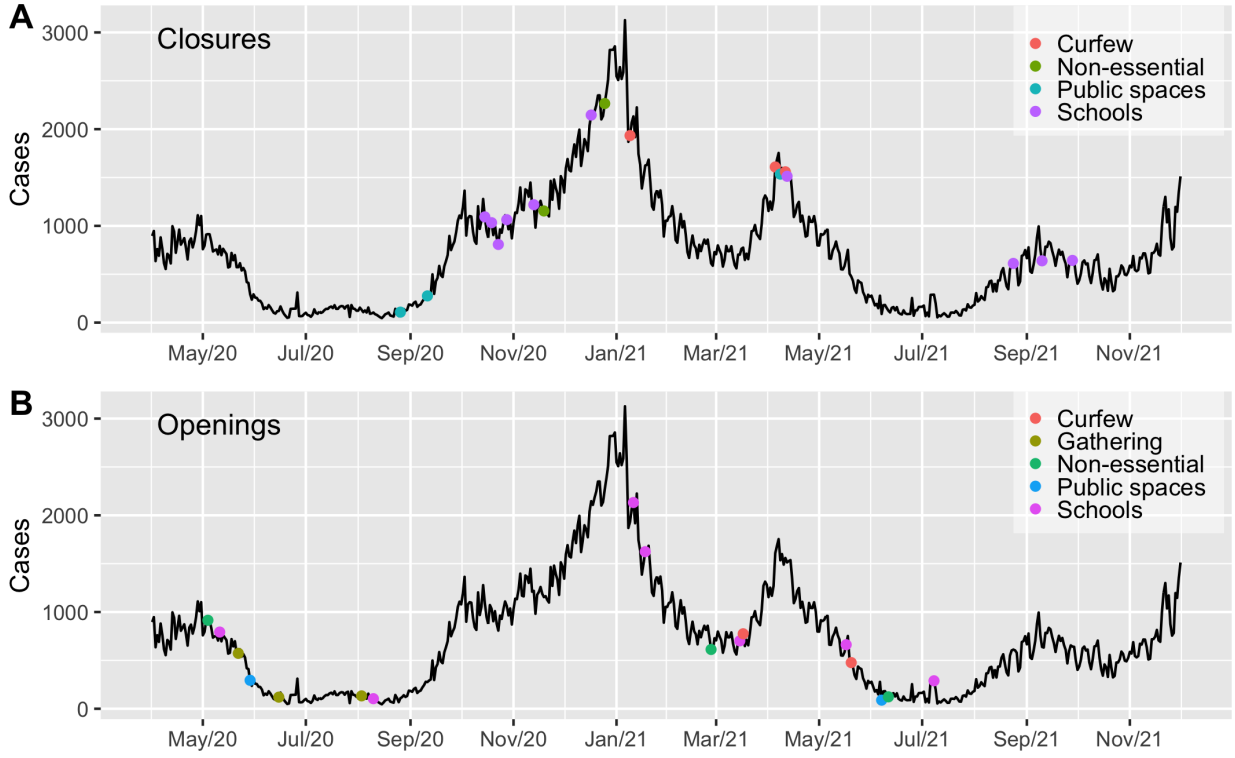

Figure 2.4: NPIs for Québec over the period from 1 April 2020 to 1 December 2021

2.6 Actual Cases

Knowing the actual number of people who are infected with COVID-19 in Canada is an essential step towards understanding the spread of the disease. In this thesis, we refer to this true number of infections as actual cases; it is also referred to as True New Daily Infections by many researchers [12].

The number of actual cases in Canada is likely greater than the number of reported cases. This is because individuals infected with the virus may not be detected for several possible reasons:

(i) they choose not to get tested because they are asymptomatic or only mildly symptomatic;

(ii) they are tested but the tests do not detect the virus (false-negative);

(iii) they do not have easy access to testing;

(iv) they simply do not want to get tested.

Contrary to the second point, there are also false-positive cases. Such cases occur when healthy individuals are tested as positive for the disease. While this leads to an overestimation of the number of cases, this impact is considered negligible. In this section, we compare two methods to estimate the actual cases from reported cases. The first is the prevalence ratio method developed in 2020 by Gu [12]. The second method is the Richardson–Lucy deconvolution algorithm [10].

2.6.1 Prevalence Ratio

Gu developed a method to estimate actual cases in the United States using the prevalence ratio, i.e., the ratio of actual cases to reported cases. Denote the prevalence ratio by ρ; it can be approximated by

$$\rho(t) = a{p_t}^b + c,$$

where t denotes the number of days since 1 March 2020, also referred to as `day_i` in Gu's paper. Here, p_t is the positivity rate for day t, and a, b, c are constants selected by Gu in a trial-and-error manner so that the estimated case curve is as close as possible to the reported case curve.

Because the epidemic situation and demographic structure are comparable for Canada and the United States, those constants may be applied to our scenario. Plugging in the values that Gu derived, viz., $a = 1500/(t + 50), b = 0.5, c = 2$, we have

$$\rho(t) = \frac{1500}{t + 50} {p_t}^{0.5} + 2,$$

where t is the number of days since 1 March 2020, and p_t is the positivity rate, the probability that an individual being tested was infected. For each province, it was calculated using the number of confirmed cases divided by the number of individuals tested. The

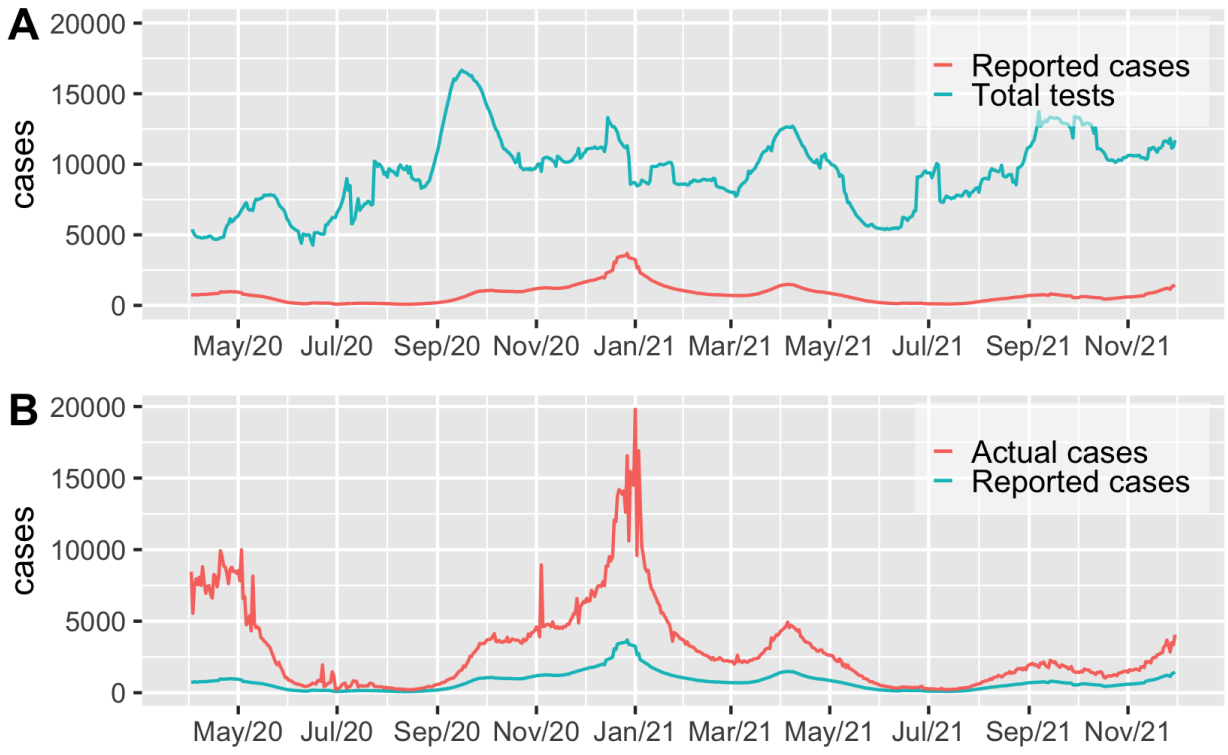

Figure 2.5: A. Actual cases vs. total tests in Québec; B. Actual cases vs. reported cases in Québec over the period from 1 April 2020 to 1 December 2021

t!]

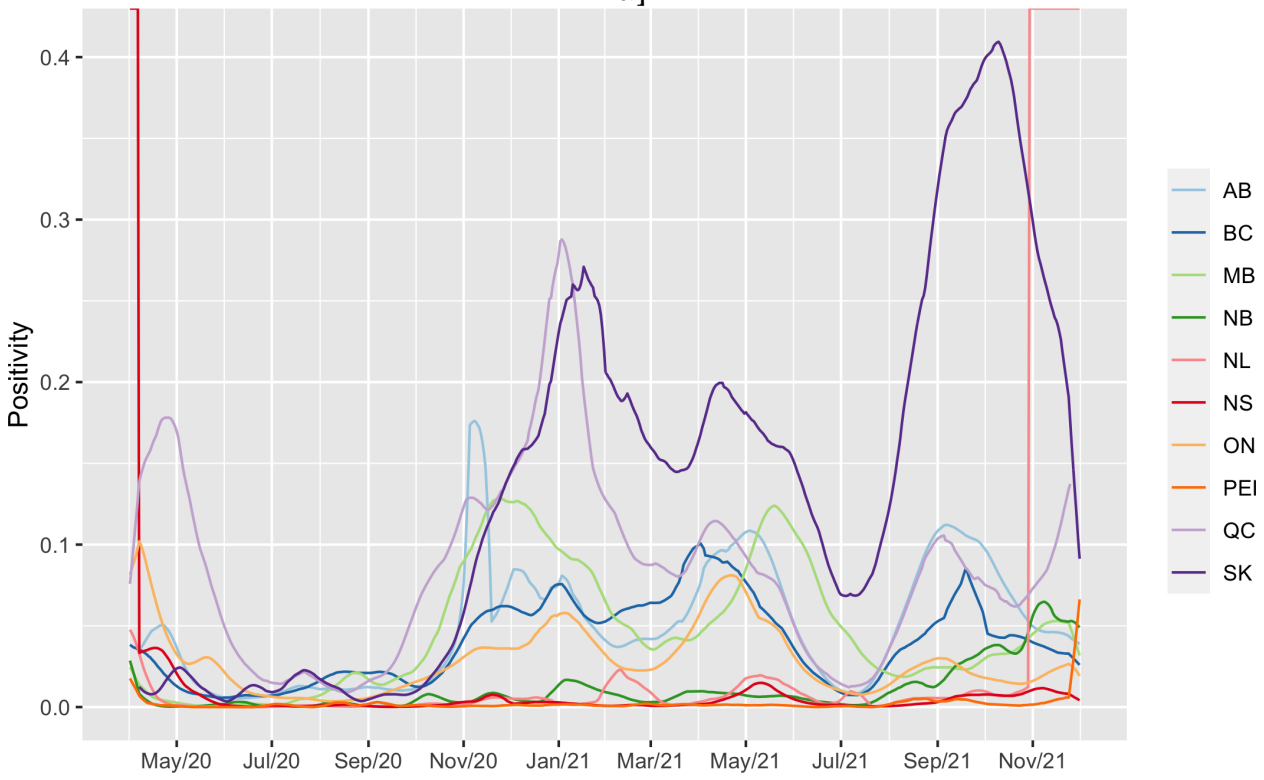

Figure 2.6: The positivity rate for each province in Canada over the period from 1 April 2020 to 1 December 2021

higher the positivity rate, the more likely it leads to the scenario of not conducting enough tests to find all the available cases, i.e., the more actual cases there should be. As the positivity rate increases, the true prevalence increases in a region relative to the reported cases. Therefore, the actual number of cases can be estimated by

$$A_t = I_t \rho(t),$$

where t is the number of days since 1 March 2020.

There is a general trend in Figure 2.6. The Atlantic provinces had a higher positivity rate at the beginning of the pandemic, whereas provinces west of Québec had a higher positivity rate around January 2021. Québec looks like the mix of those two trends. It

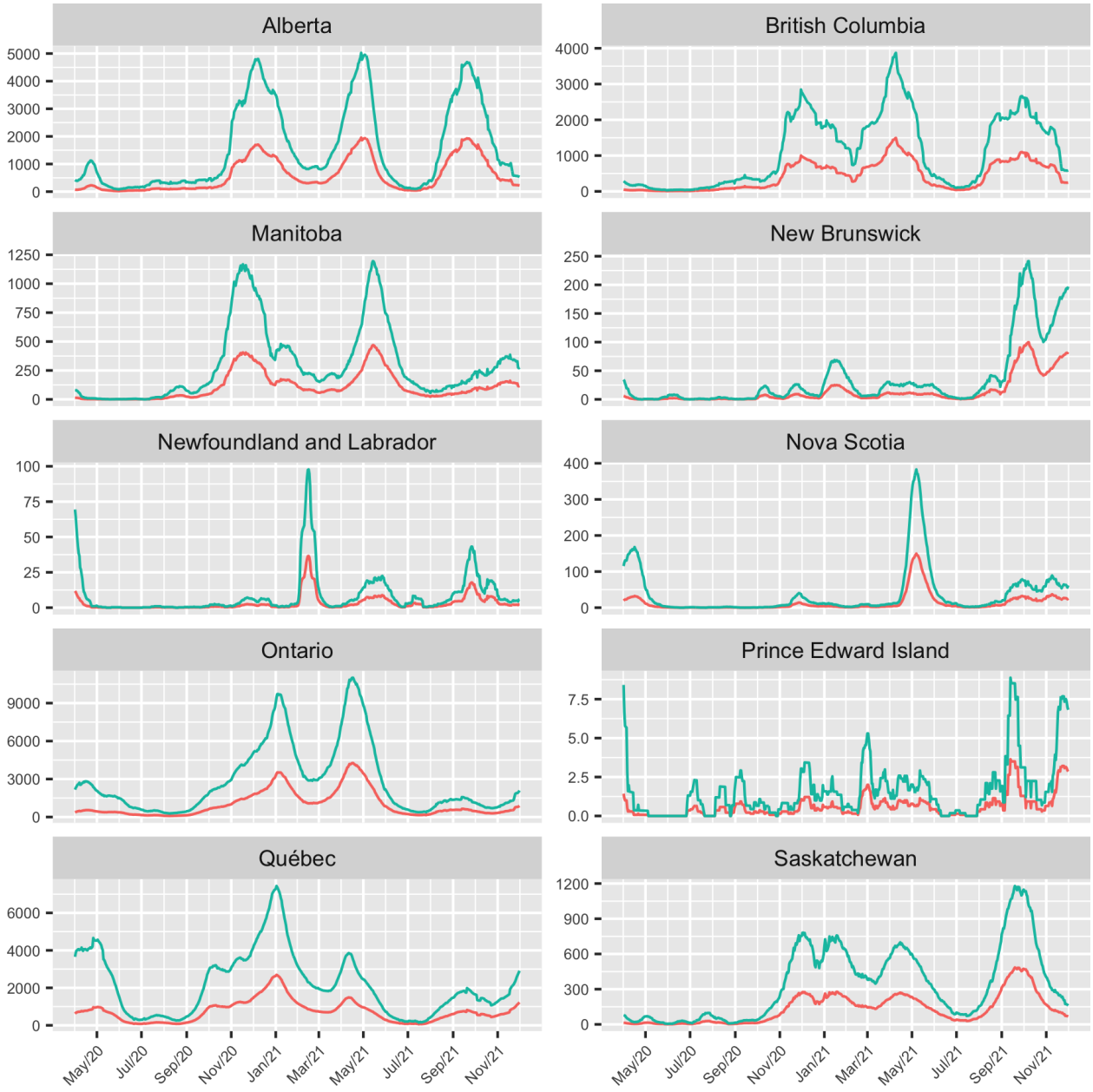

Figure 2.7: Adjusted (red) vs. reported cases (blue) for each province in Canada over the period from 1 April 2020 to 1 December 2021

reflects what happened in reality. In particular, as reported in the news, the positivity rate in the Atlantic provinces remained low for a long period.

The red and blue lines in Figure 2.7 reflect adjusted and reported cases, respectively. As shown in Figure 2.7, the actual number of cases is higher than the number of reported cases for all the provinces.

2.6.2 Richardson–Lucy Deconvolution Algorithm

The goal of the Richardson–Lucy deconvolution algorithm [10] is to reconstruct the daily actual cases A_t given the daily deaths $D_1, \ldots, D_N$ and the time-from-infection-to-death probability distribution $(d_1, \ldots, d_\ell)$, where d_k is the probability that an infected individual who will eventually die on day k after the infection.

Table 2.2 summarizes the notations used in this section. Given I_j, the reported infections on day j, let $D_{\bullet,j}$ be the total deaths resulting from infections on day j, i.e., the number of people who were infected on day j and later died. Assuming a universal infection fatality ratio ϕ, and that the number of deaths does not depend on the number of deaths on previous days, it follows that

$$D_{\bullet,j} \sim \text{Bin}(I_t, \phi).$$

Let X_{ij} be the deaths on day i due to infections on day j. The Poisson Limit Theorem [4] states that the Poisson distribution may be used as an approximation to the binomial distribution, under the conditions that the sample size, n, is large and the probability of success, p, is small.

Table 2.2: List of parameters used in the Richardson–Lucy Deconvolution Algorithm

Notation	Description	Domain
A_t	Actual total number of cases on day t	$t \in \{1, \ldots, N\}$
I_t	Observed total number of cases on day t	$t \in \{1, \ldots, N\}$
X_{ij}	Number of deaths on day $i < j$ resulting from infections on day j	$j \in \{2, \ldots, N\}$
$D_{\bullet,j}$	Observed total deaths resulting from infections on day j	$j \in \{i, \ldots, N\}$
D_t	Observed total number of deaths on day t	$t \in \{1, \ldots, N\}$
s_i	Time between the onset of symptoms in a primary case and the onset of symptoms in secondary cases	
w_i	Distribution of the daily probability of an individual becoming infectious after being infected	
d_t	Delay distribution from infection to death	
ϕ	Universal infection fatality rate (IFR)	

According to the Poisson Limit Theorem, the distribution of X_{ij} can be approximated by the Poisson distribution, viz.

$$X_{ij} \sim \mathcal{P}(\lambda_j p_{ij}),$$

where

$$p_{ij} = d_{i-j}\mathbf{1}_{j<i<j+\ell}(i).$$

In the situation where I_t is large and ϕ is small, by the Poisson limit theorem, X_{ij} can be approximated by a Poisson variable $\mathcal{P}(\lambda_t)$ with $\lambda_t = \phi I_t$. The unknown parameters $(\lambda_{1-\ell}, \ldots, \lambda_{N-1})$ can thus be estimated by iterating in the space of parameters using the expectation maximization (EM) algorithm. As the realization of the random vector $(D_1, \ldots, D_N)$ is observed while the latent random variables $X_{i,j}$ are unobserved, this process essentially amounts to using an EM algorithm with missing data. We can thus get λ_j^{r+1} from the following EM algorithm steps:

(i) Log-likelihood:

$$\begin{aligned}\ell(\lambda; D, X) &= \sum_j \sum_i \{-\lambda_j p_{ij} + x_{ij}(\ln \lambda_j + \ln p_{ij}) - \ln(x_{ij}!)\} \\ &\propto \sum_j \sum_i \{-\lambda_j p_{ij} + x_{ij} \ln(\lambda_j)\}.\end{aligned}$$

(ii) Expectation:

$$\begin{aligned}\mathbb{E}_X\{\ell(\lambda)|\lambda^{(r)}, D\} &\propto -\sum_j \sum_i \lambda_j p_{ij} + \sum_j \sum_i \mathbb{E}\{X_{ij}|\lambda^{(r)}, D\} \ln(\lambda_j) \\ &= -\sum_j \sum_i \lambda_j p_{ij} + \sum_j \ln(\lambda_j) \sum_i \sum_{x_{ij}=0}^{d_i} x_{ij} \binom{d_i}{x_{ij}} \\ &= -\sum_j \sum_i \lambda_j p_{ij} + \sum_j \ln(\lambda_j) \sum_i d_i \frac{\lambda_j^{(r)} p_{ij}}{\sum_j \lambda_j^{(r)} p_{ij}} \\ &= -\sum_j \sum_i \lambda_j p_{ij} + \sum_j \lambda_j^{(r)} \ln(\lambda_j) \frac{\sum_i d_i p_{ij}}{\sum_j \lambda_j^{(r)} p_{ij}}\end{aligned}$$

(iii) Maximization:

Let

$$\frac{\partial \ell}{\partial \lambda_j} = -\sum_i p_{ij} + \frac{\sum_j \lambda_j^{(r)} \dfrac{\sum_i d_i p_{ij}}{\sum_j \lambda_j^{(r)} p_{ij}}}{\sum_i p_{ij}} = 0.$$

Then

$$\lambda_j^{(r+1)} = \frac{\sum_j \lambda_j^{(r)} \dfrac{\sum_i d_i p_{ij}}{\sum_j \lambda_j^{(r)} p_{ij}}}{\sum_i p_{ij}}.$$

If we denote

$$q_j = \sum_i p_{ij}, \quad d_i^{(r)} = \sum_j \lambda_j^{(r)} p_{ij},$$

then

$$\lambda_j^{(r+1)} = \frac{\lambda_j^{(r)}}{q_j} \sum_i \frac{d_i p_{ij}}{d_i^{(r)}}.$$

Given a cutoff of 10 days for the infectivity process [10], the infectiousness profile distribution is $(w_1, \ldots, w_{10})$, where each w_i represents the proportion of the cumulative infectiousness which falls between days $i - 0.5$ and $i + 0.5$ for an average person.

Therefore, the infectivity ratio IR_t on day t measures the number of people infected by an "average" infector on day t, viz.

$$\mathrm{IR}_t = \frac{I_t}{\sum_{i<t} I_i w_{t-i}}.$$

The actual cases can be estimated by

$$A_t = \mathrm{IR}_t \sum_{i=1}^{10} A_{t-i} w_i.$$

Suggestion for INSPQ

The Institut national de santé publique du Québec (INSPQ) [16] used the algorithm due to Cori et al. [7] to calculate the instantaneous R_t, which incorporates the Richardson–Lucy deconvolution in R Studio Software. INSPQ first smoothed the cases curve using

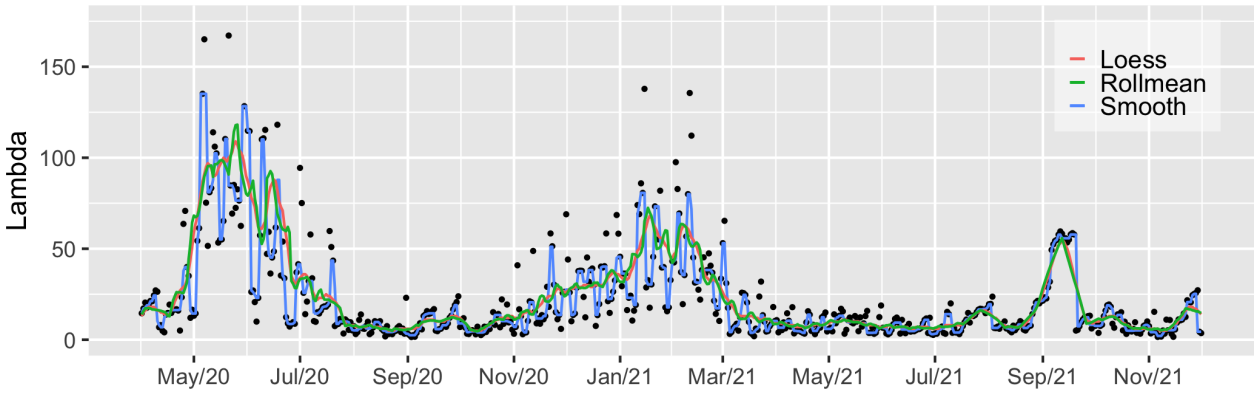

Figure 2.8: Comparison between different smoothing methods for λ for Québec data over the period from 1 April 2020 to 1 December 2021

the `loess` method. This thesis proposes to smooth the local rate parameter λ in the Richardson–Lucy algorithm rather than smoothing the data.

A comparison of λ smoothed by different methods was carried out with the algorithms set to their default configuration. The following functions were used:

(i) `approx`: linear approximation;

(ii) `smooth`: Tukey's running median;

(iii) `loess`: local weighted regression;

(iv) `rollmean`: moving average.

As can be seen in Figure 2.8, the smoothed λ from the `loess` method is less wiggly and more stable.

2.6.3 Comparison

Gu's method and the Richardson–Lucy deconvolution are two different methods of estimating the actual cases. Figure 2.9 shows the comparison between the number of actual cases estimated from Gu's prevalence ratio method and the Richardson–Lucy deconvolution method, respectively.

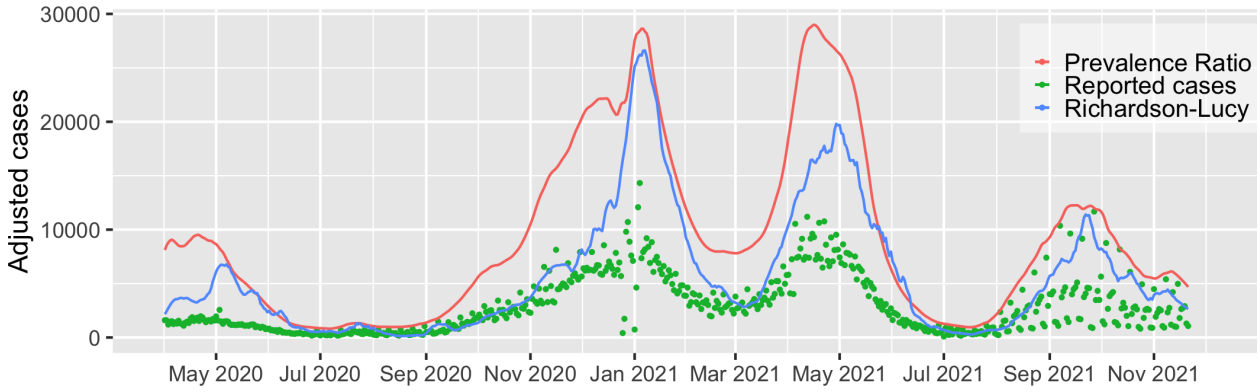

Figure 2.9: Comparison of actual cases by prevalence ratio and Richardson–Lucy deconvolution over the period from 1 April 2020 to 1 December 2021

The cases derived from Gu's method have a higher peak compared to the reported cases and have an overall trend of higher case counts, likely because they are adjusted by the positivity rate, which is larger when there are more infections. Cases from the Richardson–Lucy method have a steeper rise and a later start compared to those based on Gu's method.

Around December 2021, there was an outbreak caused by the Omicron variant, and there were not enough tests to give an accurate positivity rate. Therefore, Gu's method could be misleading because it relies heavily on the positivity rate. As a result, this thesis adopts the estimation of actual cases based on the Richardson–Lucy method.

Chapter 3

Effective Reproduction Number

Assessing the efficacy of NPIs in mitigating the spread of COVID-19 is crucial for informing future preparedness response plans. Quantifying the impact of NPIs is a crucial first step for analyzing their efficacy. As discussed in the previous chapter, the effective reproduction number, R_t, is a preeminent indicator of NPI impact.

The effective reproduction number, R_t, tracks the number of other people a single infected person is likely to infect. Changes in R_t can detect changes in the level of transmission of an infectious agent over time. An R_t greater than 1 indicates an exponential acceleration in transmission, while an R_t less than 1 indicates that the epidemic is receding. When R_t is near 1, the transmission and the number of cases remain stable. If the infection is well controlled (i.e., few cases) and an outbreak is observed, R_t will increase.

The monitoring of R_t over time provides feedback on the effectiveness of NPIs and on the need to intensify control efforts, given that the goal of such efforts is to reduce R_t below the threshold value of 1 and as close to 0 as possible, thus bringing an epidemic under control. By tailoring and optimizing interventions to keep R_t below 1, the spread of COVID-19 can be reduced.

The most prominent approach for estimating R_t is the `EpiEstim` method of Cori et al. [7]. There are alternative methods for calculating the reproduction rate, but the instantaneous R_t method is the most robust for obtaining near-real-time estimates [11].

3.1 The EpiEstim Method by Cori et al.

The `EpiEstim` technique of Cori et al. [7] is extensively used and provided as a library in R Studio Software [10, 16]. This methodology requires two types of data: (i) the epidemiological curve of new infections and (ii) the generational interval (the average time between infection of a primary case and that of a secondary case).

3.1.1 EpiEstim Algorithm

Following the setup of the Richardson–Lucy deconvolution method in Section 2.6.2, R_t is estimated using the infectivity ratio IR_t. Given a cutoff of 10 days for the infectivity process, the infectiousness profile distribution is $(w_1, \ldots, w_{10})$, where each w_i represents the proportion of the cumulative infectiousness which falls between days $(i - 0.5, i + 0.5)$ for an average person.

Therefore, the infectivity ratio IR_t on day t measures the number of people infected by an average infector on day t, viz.

$$\mathrm{IR}_t = \frac{I_t}{\sum_{i<t} I_i \, w_{t-i}}.$$

Because the number of infected individuals is large, one can compute R_t on day t in a "forward-looking" way by summing up the numbers of infections caused in subsequent days by an average person who got infected on day t, viz.

$$R_t = \sum_{i>0} \mathrm{IR}_t \, w_i = \sum_{i>0} \frac{w_i \, I_{t+i}}{\sum_{\ell=i-10}^{i-1} w_{i-\ell} \, I_i \, w_{t+\ell}}.$$

3.1.2 Effective Reproduction Number From INSPQ

The Institut national de santé publique du Québec (INSPQ) [16] used the algorithm developed by Cori et al. [7] to compute the instantaneous R_t from the number of reported cases of COVID-19 in Québec. The INSPQ is a reference centre that assists in NPI imple-

mentation decision-making in Québec. Because this thesis is focused on Québec data, it is beneficial to investigate its R_t estimation process.

The INSPQ used the `EpiEstim` package in R Studio Software to estimate R_t from epidemic curves over a five-day rolling window. Because it is uncertain on which day a person is infected, INSPQ calculated the infection curve retroactively from the time series of confirmed cases in the laboratory (date of sampling) or by epidemiological link (date of declaration).

This time series is first smoothed to reduce the impact of the effects of weekends during which a lower number of cases is generally reported. The smoothed series is then used to calculate the infection curve from a Richardson–Lucy type deconvolution algorithm which enables infection times to be estimated.

Figure 3.1 shows the comparison of R_t from INSPQ and from the state-space model with a seven-day window. INSPQ estimated R_t using a five-day window. Because the first publicly accessible R_t from INSPQ is on 1 July 2020, the figure contains data from 1 July 2020 to 1 December 2021.

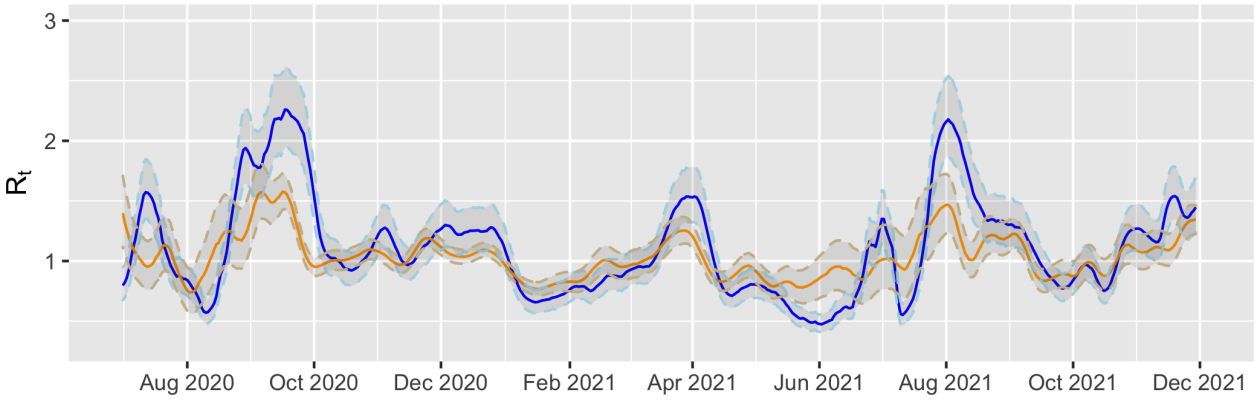

Figure 3.1: Comparison of R_t from INSPQ (yellow) and from the state-space model (blue) with a five-day window

3.1.3 Method Verification

An essential step before simulating R_t to analyze the impact of NPIs is to validate the methodology. Many researchers use the `EpiEstim` package in R Studio software to simulate R_t from daily infections data (Goldstein et al. [10], INSPQ [16]). However, it is unknown whether the wiggly R_t curves are real or just a feature of the estimation.

It is crucial to understand the sensitivity of the `EpiEstim` when generating R_t from infections. One way to test it is to create a scenario where `EpiEstim`'s R_t should be a time series sequence of the same value, which is constant. Infections data with a known R_0 were simulated and inputted to the `EpiEstim` function. The `EpiEstim` function should generate a fixed R_t of the value R_0. If the R_t generated is wiggly under these conditions, we can conclude that it is a feature of estimation due to the `EpiEstim` algorithm.

We inputted constant case counts into the `estimate_R` function in `EpiEstim` to estimate R_t; the latter was expected to be a constant function at level 1. However, the estimated R_t is not constant. Rather, it starts at a high value, fluctuates and converges to 1 no matter what case counts are inputted.

As `estimate_R` is a widely used algorithm, further validation was warranted. In particular, we scrupulously investigated the nature of the requested parameters.

Poisson Regression

After careful investigation of the study of Cori et al. [7], we clarified that the `EpiEstim` function requires that the input cases follow a Poisson regression model. We were unable to reproduce a constant R_t from the simulated cases in Section 3.1.3 because we did not follow this requirement. Therefore, we constructed a Poisson regression model to simulate case counts using R Studio Software. The notations used in this section are described in Table 2.2. R studio's `rpois` function generates random counts from the Poisson distribution and returns the results. The function takes two arguments: number of random values to return, and λ, which is the estimated rate of events for the distribution; this is expressed as average events per period.

It is of interest to see how well this algorithm responds to transitions in R_t. As a result, we ran a simulation in which we artificially constructed an R_t series, generated cases using Poisson regression using this series, and then reestablished an R_t series using `EpiEstim`. We expected the algorithm to generate the same R_t series that we provided.

We defined the serial interval to be probabilities $w_1, \ldots, w_t$ (summing to 1) describing the average infectiousness profile after infection. We set R_t to be 1.5 for the first 150 days and 0.8 for the next 150 days. The total number (N) of days was chosen to be 300. We simulated the serial interval w using a Gamma distribution with mean $\mu_w = 7$ and standard deviation $\sigma_w = 1.1$. These values were selected for illustration purposes and could be adjusted in accordance with real-world scenarios.

Therefore, the incidence at time t follows a Poisson distribution with mean λ_t, where for all $t \in \{2, \ldots, N\}$,

$$\lambda_t = \sum_{s=1}^{t} R_t I_{t-s} w_s.$$

In the defined scenario, this formula can be specified as

$$\lambda_t = \begin{cases} \sum_{s=1}^{t} 1.5\, I_{t-s}\, w_s & \text{for the first 150 days,} \\ \sum_{s=1}^{t} 0.8\, I_{t-s}\, w_s & \text{for the next 150 days.} \end{cases}$$

Figure 3.2 suggests that the R_t estimated by `EpiEstim` approximately agrees with the simulated R_t we input into the function, which is 1.5 for the first 150 days and 0.8 for the next 150 days. We also tested when R_t remains constantly 1.5, and obtained a roughly constant estimate of 1.5 after the regression. Remarkably, there are slight fluctuations at the beginning of the fit. We may conclude that the R_t's wiggly curves are a feature of the estimation. Section 3.2 indicates some implications of this feature. Particularly, Section 3.2.2 illustrates how this seemingly innocuous inaccuracy in the estimation process may lead to false conclusions.

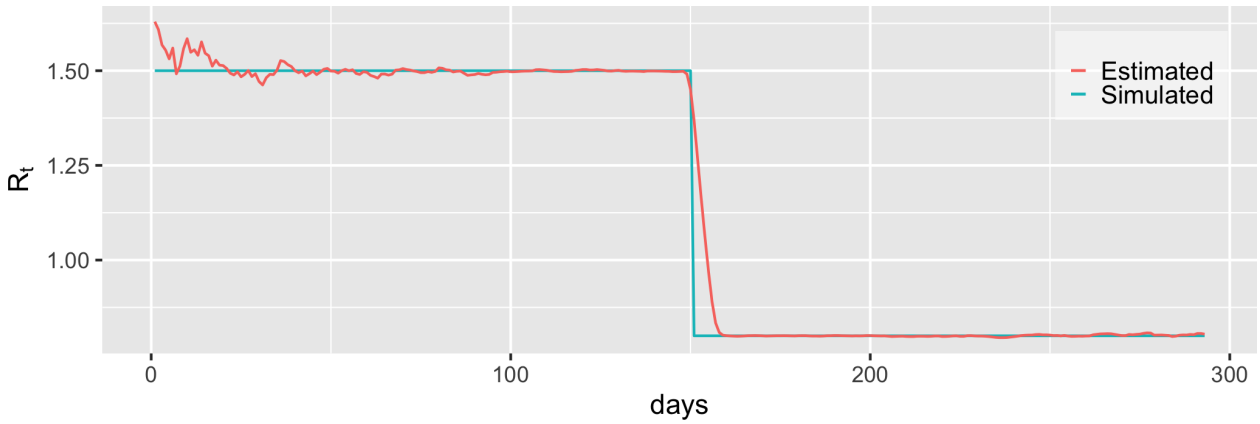

Figure 3.2: Comparison of the simulated R_t and R_t estimated by `EpiEstim` over time

3.2 Challenges

A confidence interval measures the degree of uncertainty in a sampling method and provides a range of values that could contain the true population mean. An appropriate confidence interval can provide an adequate representation of reality while accounting for methodological inaccuracies in estimating.

There are three factors that generally influence the size of the confidence interval:

(i) the size of the sample;

(ii) the variability of the sample;

(iii) the confidence level: how much to trust the confidence-interval calculation.

In general, narrower confidence intervals carry more information. Researchers usually strive for tight confidence intervals while conducting quantitative research. A common pitfall many researchers overlook in the estimation of R_t is the derivation of a corresponding confidence interval. Without a carefully calculated confidence interval, a hasty analysis could misinterpret the natural variation of R_t as the impact of NPIs.

3.2.1 Weakness of the EpiEstim Algorithm

There is no doubt that the algorithm of Cori et al. [7] made substantial contributions to many fields and made many studies possible. While it is worth acclaiming that the algorithm of Cori et al. [7] incorporates a great effort in attempting to achieve a narrow confidence interval, there are certain downsides to the algorithm.

The approach of Cori et al. [7] fails to address two major concerns, resulting in an improper representation of uncertainty. First, the confidence interval lacks statistical significance because the method is deterministic. Second, the likelihood calculation for the aggregated data relies on the premise of independence between time points.

With regard to the confidence interval lacking statistical significance, one factor that influences the size of the confidence interval is the variability of the sample. However, we argue that the algorithm of Cori et al. [7] does not address the right kind of variability. This method ties the confidence interval too closely to the single accessible dataset; it has induced dependence between successive posteriors, which reduces variability. The confidence interval must account for variations across datasets. A proper Bayesian strategy necessitates the collection of cross-dataset variability.

As for the second concern, the likelihood calculation for the aggregated data is based on the assumption of independence between time points. According to Cori et al. [7], the `estimate_R` function is suitable for handling non-smooth data. The non-smoothness comes from the weekend effect [6], given that Saturday and Sunday's cases were reported on Monday. Cori et al. [7] stated:

> "However, the resulting R_t estimates can be highly variable and hence difficult to interpret when the time step of data is small. We therefore calculate estimates over longer time windows, under the assumption that the instantaneous reproduction number is constant within that time window." [7], p. 1

Cori et al. [7] provided an example of smallpox in Kosovo in 1972, in which the daily estimates of R_t were plotted for one-day, one-week, two-week, and four-week windows, assuming a known serial interval distribution. It was found that

> "The estimates varied substantially according to the window size chosen. The one-day window estimates were so variable that it was hard to derive any trend from them. As the window size grew, the median estimates were smoother, and the credible intervals were narrower, as expected." [7], p. 4.

Cori et al. [7] model transmission with a Poisson process, so that the rate at which someone infected in time step $t - s$ generates new infections in time step t, is equal to $R_t w_s$ where w_s is a probability distribution (hence summing to 1) describing the average infectiousness profile after infection.

Therefore, the likelihood of incidence I_t given the reproduction number R_t, conditional on the previous incidences $I_0, \ldots, I_{t-1}$ is

$$\Pr(I_t \mid I_0, \ldots, I_{t-1}, w, R_t) = \frac{(R_t \Lambda_t)^{I_t} e^{-R_t \Lambda_t}}{I_t!},$$

with $\Lambda_s = I_{t-1} w_1 + I_{t-2} w_2 + \cdots + I_0 w_t$.

The calculation of this likelihood is achieved using `rpois(poisson_mean,case)`, where `poisson_mean` is the result from the `simulate_forward` function and `case` is the actual case series. Given that the `estimate_R` algorithm uses a weekly window to calculate R_t, it is necessary to calculate the aggregated likelihood, i.e., the likelihood of the incidence during a time period $[t - \tau + 1; t]$ over which the transmissibility is assumed constant, measured by the reproduction number $R_{t,\tau}$.

Cori et al. [7] derived the likelihood of the incidence during this time period, viz. $I_{t-\tau+1}, \ldots, I_t$ given the reproduction number $R_{t,\tau}$, conditional on the previous incidences $I_0, \ldots, I_{t-\tau}$ to be

$$\Pr(I_{t-\tau+1}, \ldots, I_t \mid I_0, \ldots, I_{t-\tau}, w, R_{t,\tau}) = \prod_{s=t-\tau+1}^{t} \frac{(R_{t,\tau} \Lambda_s)^{I_s} e^{-R_{t,\tau} \Lambda_s}}{I_s!}. \tag{3.1}$$

Cori et al. [7] found that the posterior distribution of $R_{t,\tau}$ is Gamma with parameters

$$\left(a + \sum_{s=t-\tau+1}^{t} I_s, \frac{1}{1/b + \sum_{s=t-\tau+1}^{t} \Lambda_s}\right)$$

where a and b represent the shape and scale parameters for the Gamma distribution, respectively. In particular, the posterior mean of $R_{t,\tau}$ is

$$\frac{a + \sum_{s=t-\tau+1}^{t} I_s}{1/b + \sum_{s=t-\tau+1}^{t} \Lambda_s},$$

and the standard deviation of $R_{t,\tau}$ is

$$\frac{\sqrt{a + \sum_{s=t-\tau+1}^{t} I_s}}{1/b + \sum_{s=t-\tau+1}^{t} \Lambda_s}.$$

Critical to the expression of (3.1) is the assumption that the conditional incidences are independent, which is unreasonably restrictive for many real-world data-generating processes. The likelihood obtained from Cori et al.'s method is suboptimal because it assumes independence of time points; it reconstructs Λ_s every time, which is suitable for a point estimate but it is likely to be a misrepresentation for a whole time span. The so-called likelihood after aggregating a seven-day window is no longer a likelihood and would cause an improper representation of uncertainty.

Cori et al. [7] observed that as the window size grew, the median estimates were smoother, and the credible intervals were narrower.

The solution to this problem is to get rid of independence by generating new incidences. Section 3.3 proposes to use the state-space model to emulate samples. The advantage of this emulation method is that it generates independent samples, allowing us to estimate the confidence interval based on cross-dataset variability. This emulation method is the proper Bayesian representation of uncertainty.

3.2.2 Synthetic Effective Reproduction Number

A serious ramification of the absence of a proper confidence interval is that it is unable to detect the nature of changes in R_t, resulting in biased conclusions drawn from such analyses. It is of interest to check whether the changes in R_t are in response to the implementation of NPIs. Does R_t change as a response to NPIs, or is it possible that the fluctuations in R_t are merely the product of its natural variation?

To further analyze the pattern of the changes in R_t, a synthetic cases curve with randomly generated R_t was constructed. Each R_t is defined to be the sum of $0.9\, R_{t-1}$ and the randomly generated ϵ, where $\epsilon \in (0, 0.1)$.

The serial interval was generated using a Gaussian distribution with mean $\alpha = 7$ and standard deviation $\beta = 1.1$. Using similar bootstrap techniques, the confidence intervals for the synthetic R_t and a curve of cases were acquired.

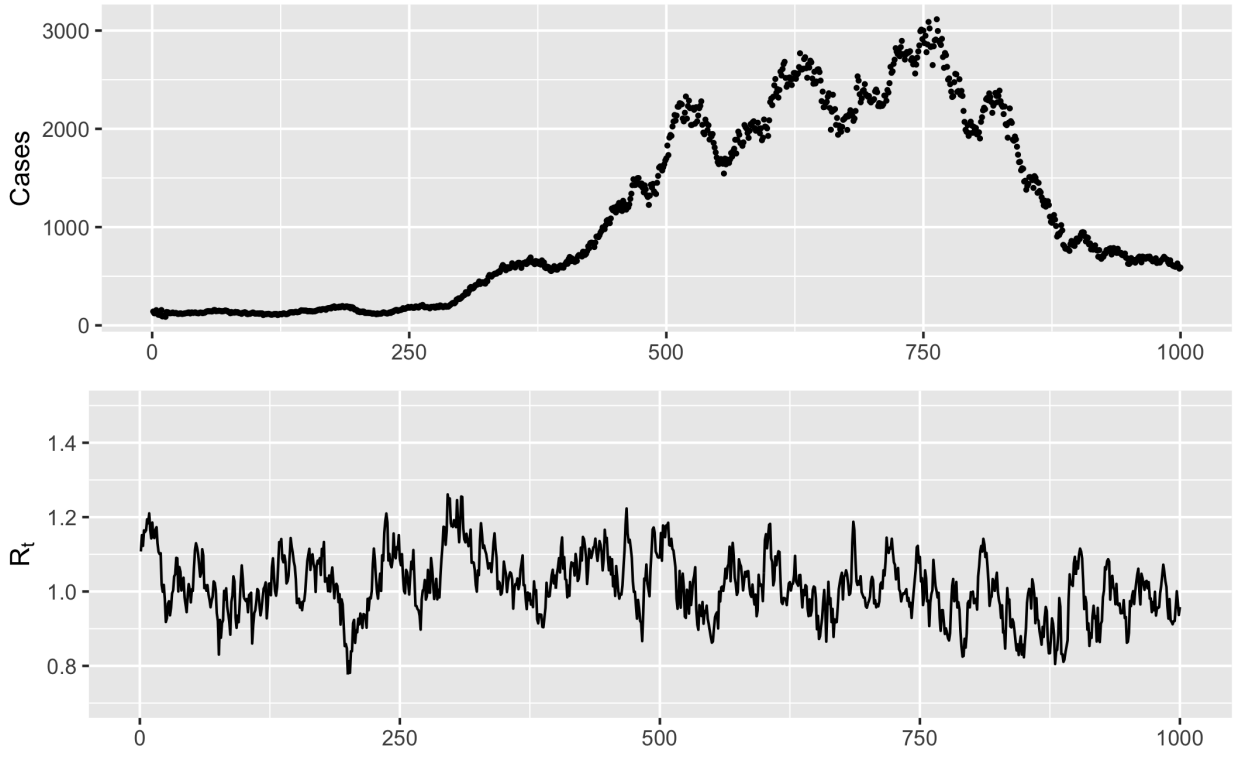

Figure 3.3: Synthetic cases and R_t with randomly generated, normally distributed R_t

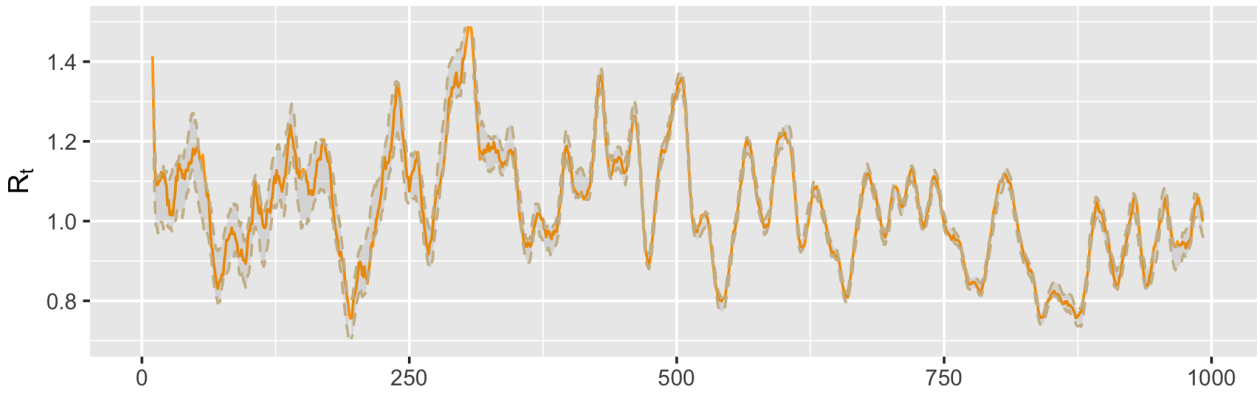

Figure 3.4: R_t from simulation-based method with 2000 iterations for a seven-day window

Figure 3.3 shows that it is possible to construct a cases curve from randomly generated, normally distributed R_t. That is, there is a natural fluctuation of R_t of around 0.8 to 1.2.

Figure 3.4 shows that the R_t from the algorithm developed by Cori et al. [7] has a very narrow confidence interval with 2000 iterations for a seven-day window. This exercise illustrates that the cases can be reconstructed from a synthetic R_t, implying that the changes in R_t are natural fluctuations rather than reflections of the NPIs.

Because the confidence interval estimated using the method of Cori et al. [7] is too narrow, one can mistakenly interpret changes in R_t as a reflection of the NPIs, leading to incorrect conclusions.

To reach a reasonable judgment about the effect of NPIs, one must carefully examine R_t and a corresponding confidence interval. This thesis proposes a statistically rigorous method to solve this problem.

3.3 Simulation and Emulation-Based Analysis

A weakness of the `EpiEstim` methodology is that it is deterministic, meaning that the `EpiEstim` function produces the same result given the same parameters. This leads to many problems. Most importantly, the confidence interval acquired by this method has no statistical meaning as the model is not stochastic.

Researchers have tried many ways to achieve more realistic confidence intervals. For example, some researchers acquired the confidence interval by simulating data for 5000 randomly generated sets of parameters, and keeping the 1000 closest simulations to compute what they referred to as the "confidence interval" around the mean. This process remains deterministic despite an attempt to incorporate randomness.

We developed an alternative approach to obtain a statistically meaningful confidence interval using parametric bootstrap sampling. In this approach, 2000 samples were generated and kept. The estimated trajectories of case counts give a genuine estimation of uncertainty, which is what a confidence interval is aimed at doing. We compared two methods of generating samples. The first is to perform forward-simulation using `rpois`. The second is to use a state-space model to emulate samples.

3.3.1 Forward Simulation

We developed an alternative approach to obtain a statistically meaningful confidence interval. The cases were smoothed using a seven-day moving average to offset the weekend effect [6], given that Saturday and Sunday's cases were reported on Monday.

In this approach, 2000 samples were generated and kept. The estimated trajectories of case counts give a genuine estimation of uncertainty, which is what a confidence interval is aimed at doing.

The samples were simulated from a parametric bootstrap methodology. Parametric bootstrapping assumes that the data come from a known distribution with unknown parameters; in this analysis, the data are assumed to come from a Poisson distribution. The parameters were estimated using the observed data and the estimated distributions were then used to simulate the samples.

Parametric Bootstrap Procedure

We constructed a Poisson regression model using the algorithm specified in Section 2.6.2 and denoted it as $f(\mu, \sigma, R_t)$, where μ and σ represent the mean and standard deviation

for the serial interval, respectively. It is referred to as `find_poisson_case` in R Studio, which takes R_t, `mean_w` (μ) and `var_w` (σ) as parameters.

The parametric bootstrap procedure is as follows:

1. Obtain the fitted case count and the mean and standard deviation for the serial interval μ_0 and σ_0 using the `Optim` function with objective function

$$\ell\{(C, S(w)\} = \ell\{C, f(7.1, 1.1, R_t)\}.$$

   The initial parameters 7.1, 1.1 are the results based on the actual case count of the grid search. An estimate of R_t was then obtained using `estimate_R`. Estimates of μ and σ were found using the `Optim` function. The fitted parameters as μ_0 and σ_0 are then stored.

2. Repeat the following steps K times, say $K = 2000$, as was done in this thesis:

   (i) Simulate the incidence forward using the distribution of the serial interval $w(\mu_0, \sigma_0)$ and using the `rpois` function in the Poisson mean calculation. Store the simulated incidence and denote it as S_i for the ith step.

   (ii) Obtain the optimal (μ_i, σ_i) using the `Optim` function, with cases being the simulated S_i and the initial values being $(\mu_0 + \epsilon_1, \sigma_0 + \epsilon_2)$, where ϵ_1 and ϵ_2 are the incorporated perturbations. These perturbations are random numbers generated from a uniform distribution on the interval $(-1, 1)$ for mean and $(-0.05, 0.05)$ for standard deviation.

   (iii) Estimate the R_t curve for step i using the `estimate_R` function with the simulated incidence S_i and the distribution of serial interval; the distribution of serial interval is modelled by a Gaussian regression with parameters (μ_i, σ_i).

The final step extracts the point-wise confidence interval from the simulated samples. We used the 97.5th and 2.5th values of the ranked differences as the endpoints of the 95%

confidence interval. To do that, we sorted the list of samples S_i by their loss function and used the quantile function in R Studio software.

Optimization

For each iteration in this simulation-based approach, an optimization is performed to find the fitted case curves. Let w be the distribution of serial intervals, and μ_w and σ_w be the mean and standard deviation for the Gaussian regression parameters of the serial interval, respectively. The `estimate_R` function requires the mean and variance for w to be larger than 1. In this section, w and $w(\mu_w, \sigma_w)$ will be used interchangeably. Let $i \in \{1, \ldots, N\}$ be the days, and N be the total number of days.

Define the loss function to be the sum of differences of the simulated cases S_i and reported cases I_i, viz.

$$\ell\{S(w), I\} = \sum_{i \in \{1,\ldots,N\}} \ell\{S_i(w), I_i\}.$$

The objective is

$$\min_{w(\mu_w,\sigma_w)} \ell\{S(w), I\} \quad \text{for } \mu_w, \sigma_w > 1,$$

because the `estimate_R` function requires the mean and variance for w to be greater than 1. To ensure that the parameters stay in the allowed region, a penalty M was added to transform this unconstrained problem into a constrained problem.

Therefore, the objective was taken to be

$$\min_{w(\mu_w,\sigma_w)} \ell\{S(w), I\} = \begin{cases} M & \text{if } \mu_w, \sigma_w \leq 1, \\ \sum_{i \in \{1,\ldots,N\}} \ell\{S_i(w), I_i\} & \text{if } \mu_w, \sigma_w > 1. \end{cases}$$

The constant M needs to be sufficiently large so that the algorithm would avoid taking parameters outside the designated domain; but if M is too large, the algorithm could not

escape it and would fail to work. After trial and error, this penalty M was chosen to be

$$\sum_{i\in\{1,\ldots,N\}} \ell\{S_i(w), I_i\} + \sum_{i\in\{1,\ldots,N\}} {I_i}^2.$$

Loss Functions

We tried four different types of loss functions: squared loss, and absolute loss, Huber loss, and likelihood loss. The squared loss, defined by

$$\ell\{I, S(w)\} = \sum_{i\in\{1,\ldots,N\}} \{I_i - S_i(w)\}^2,$$

has the disadvantage that it has the tendency to be dominated by outliers because the squared function enlarges differences drastically. Given that our data include outliers, this loss function was deemed inappropriate.

The absolute loss, defined by

$$\ell\{I, S(w)\} = \|I - S(w)\|_1 = \sum_{i\in\{1,\ldots,N\}} |I_i - S_i(w)|,$$

mitigates the issue with outliers. Nevertheless, the fit we obtained was not satisfactory.

The Huber loss is a more robust function that may be regarded as a compromise between the squared loss and absolute loss. It is defined by

$$\ell\{I, S(w)\} = \sum_{i\in\{1,\ldots,N\}} \begin{cases} \frac{1}{2}\{I_i - S_i(w)\}^2 & \text{if } |I_i - S_i(w)| \le \delta, \\ \delta\left[\{I_i - S_i(w)\} - \frac{1}{2}\delta\right] & \text{otherwise.} \end{cases}$$

The Huber loss parameter δ controls the influence of the outliers. The higher the value of δ, the more quadratic the fit gets, and the more weight the fit assigns to the outliers. The Huber loss is a better choice as it takes outliers into account without being dominated by them. The Huber loss fits similarly as the likelihood loss.

Because Cori et al. [7] used likelihood to estimate R_t, it is most appropriate to report the result using likelihood loss. Consequently, the likelihood loss will be used for this analysis. It is defined by

$$\ell\{C, S(w)\} = \sum_{i \in \{1,\ldots,N\}} \lambda^{S(w)} e^{-\lambda / S(w)!},$$

where the expected number of events λ equals the Poisson mean. It is realized using the `dpois` function in R Studio.

Optim

The `Optim` function in R Studio was used to find the optimal parameters that minimize the loss function. The parameters of interest are the mean μ and standard deviation σ for the distribution of the serial interval. We inputted the case counts and initial guesses of the mean and standard deviation. The algorithm simulated cases using the initial guesses and updated the parameters in a quasi-Newton manner. The optimization is based on the Broyden—Fletcher-–Goldfarb—Shanno (BFGS) algorithm [17], which does line search with the descent direction preconditioned by the gradient with curvature information.

The initial guess was chosen based on a grid search. A grid search algorithm generated four pairs of parameters from 1 to 10, by steps of 0.1. It was found that good starting values for the mean and variance for the distribution of serial interval are 7.1 and 1.1, respectively.

The case count was estimated using the `Optim` function and `estimate_R` function in R Studio Software. A statistically sound uncertainty estimate was obtained using the resulting trajectories of case counts. The `estimate_R` function takes the reported cases, the prior distribution on R_t, and the distribution of serial intervals as inputs to estimate R_t. The `Optim` function finds the parameters that minimize total cost. We then input those parameters into the Poisson regression model to simulate case counts.

The prior distribution on R_t and the distribution of serial intervals can be taken to be Gaussian distributions. We conducted a grid search and compared different researchers' parameters and decided to use 7.1 and 1.1 as the mean and standard deviation for the Gaussian prior R_t distribution, respectively. Fixing the parameters for the prior on R_t, we used the `Optim` function to find optimal parameters for the distribution of serial intervals.

3.3.2 State-Space Model

State-space models are a kind of autoregressive time series model that enables us to incorporate uncertainty in the observation model. The essential idea is that behind an observed time series X_t, there is an underlying process S_t which itself is evolving through time in a way that reflects the structure of the system being observed.

We emulated 2000 case curves with the smoothed model M in the state-space model. To estimate R_t, we used the `optim` function in R to get the parameters that maximize the likelihood of the serial interval. A statistically sound uncertainty estimate was obtained using the resulting trajectories of case counts.

It is more likely for the correlations to be spurious when time series show strong trends. Differencing a time series is a practical approach to removing trend and/or seasonality from a time series. The lag-1 differencing is useful for removing trends.

Figure 3.5 indicates some time-varying heteroscedasticity and a seven-day periodicity in the differenced data. The auto-correlation function (ACF) has confidence bands in dotted lines. Counting the lines from the left, it can be seen that every 7th lag is outside the confidence band, reflecting the periodicity. The seven-day periodicity in the data is a concern. To address this, we fitted a state-space model with a seven-day seasonal component and a random walk on the mean. For the local level model (random walk

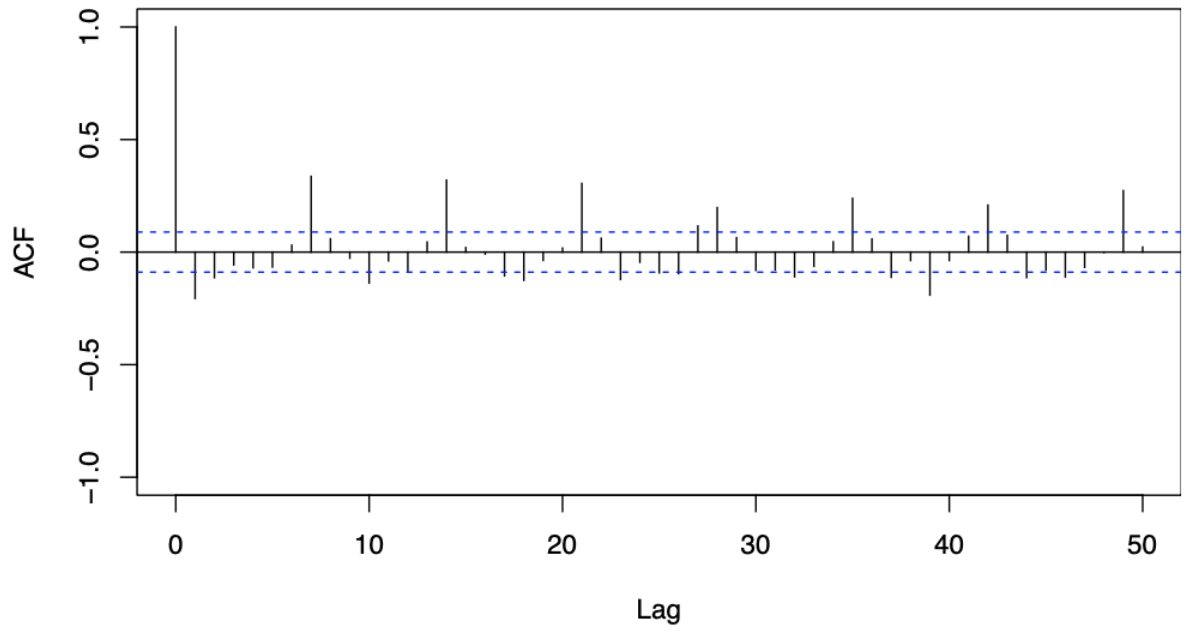

Figure 3.5: The ACF plot of the state-space model

plus noise) with a seven-day stochastic cycle, we have

$$\begin{aligned} \text{OBSERVATION EQUATION} \qquad Y_t &= M_t + S_t + V_t, \\ \text{STATE EQUATIONS} \qquad M_{t+1} &= M_t + W_{1t}, \\ S_{t+1} &= -S_t - \cdots - S_{t-5} + W_{2t}, \end{aligned}$$

where Y is the log observed count, M is the signal, S is the periodic cycle, V is the normally distributed noise for the observation variable, while W_1 and W_2 are normally distributed noise for M and S, respectively.

Thus, the state is seven-dimensional, viz.

$$\mathbf{X_t} = (\mathbf{M_t}, \mathbf{S_t}, \mathbf{S_{t-1}}, \mathbf{S_{t-2}}, \ldots, \mathbf{S_{t-5}})^\top$$

with the input matrix **F** and the state matrix **G**, where

$$\mathbf{F} = \begin{bmatrix} 1 & 1 & 0 & 0 & 0 & 0 & 0 \end{bmatrix} \qquad \mathbf{G} = \begin{bmatrix} 1 & 0 & 0 & 0 & 0 & 0 & 0 \\ 0 & -1 & -1 & -1 & -1 & -1 & -1 \\ 0 & 1 & 0 & 0 & 0 & 0 & 0 \\ 0 & 0 & 1 & 0 & 0 & 0 & 0 \\ 0 & 0 & 0 & 1 & 0 & 0 & 0 \\ 0 & 0 & 0 & 0 & 1 & 0 & 0 \\ 0 & 0 & 0 & 0 & 0 & 1 & 0 \end{bmatrix}$$

and variance matrices

$$\mathbf{V} = \sigma_{\mathbf{1}}^{\mathbf{2}} \qquad \mathbf{W} = \begin{bmatrix} \sigma_2^2 & 0 & 0 & 0 & 0 & 0 & 0 \\ 0 & \sigma_3^2 & 0 & 0 & 0 & 0 & 0 \\ 0 & 0 & 0 & 0 & 0 & 0 & 0 \\ 0 & 0 & 0 & 0 & 0 & 0 & 0 \\ 0 & 0 & 0 & 0 & 0 & 0 & 0 \\ 0 & 0 & 0 & 0 & 0 & 0 & 0 \\ 0 & 0 & 0 & 0 & 0 & 0 & 0 \end{bmatrix}.$$

Then we emulated data from the estimated model and re-estimated the R_t for each. In Figure 3.6, the blue curve represents the signal, M, where the periodicity has been removed. Figure 3.6 shows that the estimated data fit the real data well. We used the `dlmSmooth` function in R to get smoothed case curves.

To get the confidence interval, the estimated M was simulated to get 2000 datasets. Of note, those simulated datasets are now models rather than data. Then, the `estimate_R` was used to estimate R_t from those models, and the confidence interval was computed using these R_t estimates.

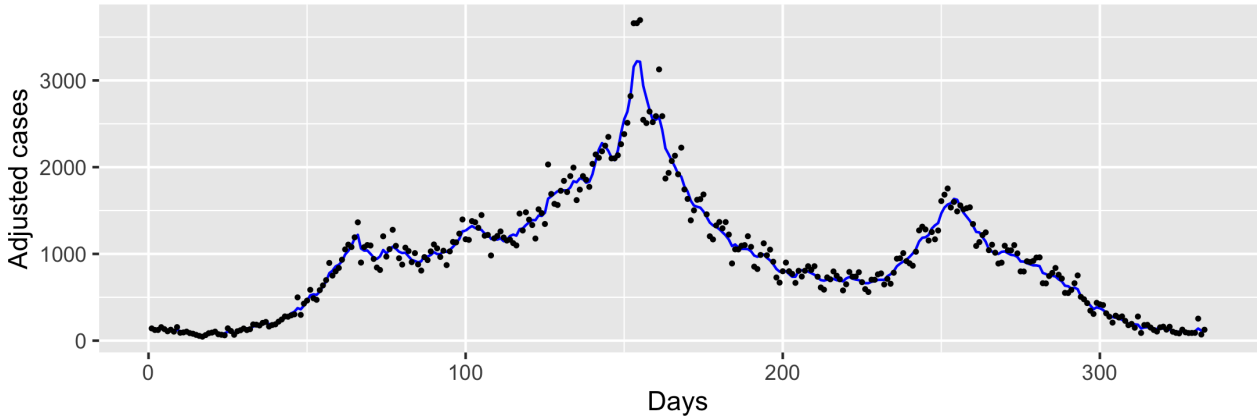

Figure 3.6: Random walk plus noise (smoothed state) plot

3.3.3 Result

As discussed in Section 3.2, the algorithm of Cori et al. [7] does not address the right kind of variability. The solution to the likelihood aggregation problem is to get rid of independence by simulating new incidences. We decided to use the state-space model to emulate samples. The advantage of this approach is that it generates independent samples, so that independence across time is no longer necessary. This method gives a statistically sound estimation of uncertainty and, as a result, a broader confidence interval.

Panel A of Figure 3.7 shows the estimated confidence interval for reported cases in Québec over the period from 1 April 2020 to 1 December 2021 on a seven-day window, based on the Monte Carlo method with samples emulated by the state-space model with 2000 iterations.

Panel B of Figure 3.7 illustrates, for the same period and window, the reproduction number R_t and a corresponding confidence interval estimated using the Monte Carlo method with samples emulated by the state-space model with 2000 iterations. It is worth noting that around September 2020, the confidence interval for R_t is very narrow. This is possibly because the increase was very rapid.

The comparisons of R_t for the two provinces for window sizes 1, 5, 7, and 14 of the same scale are available in Section A.4 in the Appendix. The results for the seven-day

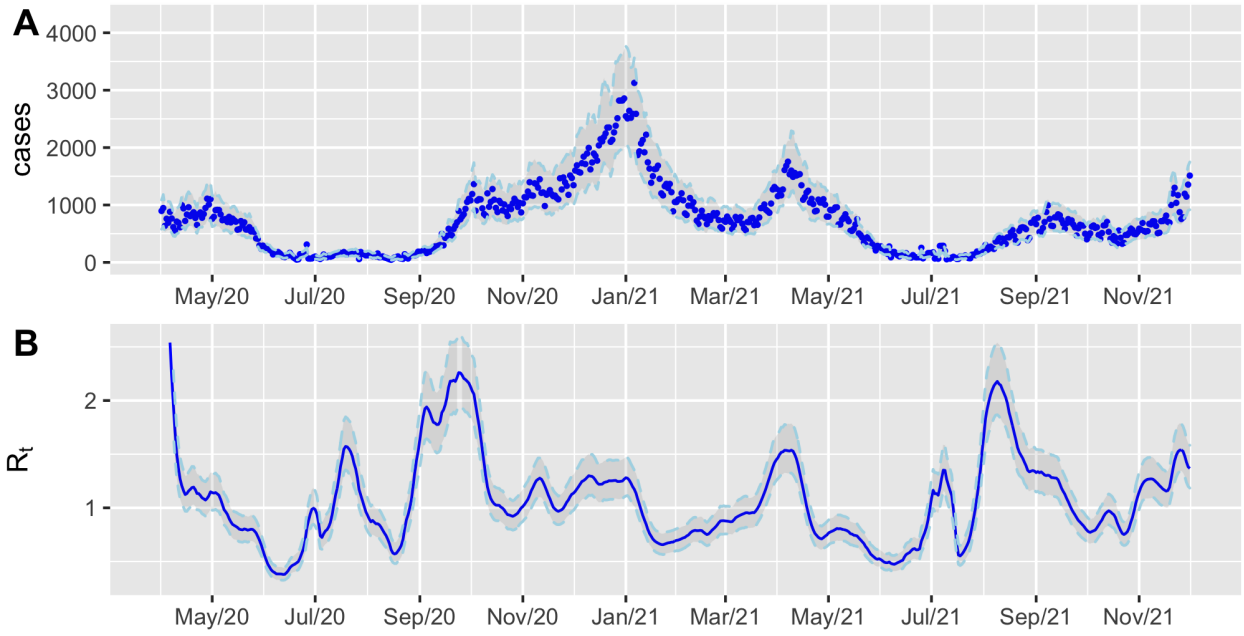

Figure 3.7: A. Reported cases and estimated confidence interval in Québec over the period from 1 April 2020 to 1 December 2021. B. R_t and the estimated confidence interval over the period from 1 April 2020 to 1 December 2021

window and five-day window are very similar. We decided to use the seven-day window as it offsets the weekend effects.

Panel A of Figure 3.8 shows R_t and its estimated confidence interval using `EpiEstim` over the period from 1 April 2020 to 1 December 2021. The confidence interval in panel A is significantly narrower than in panel B. It is not convincing that R_t fluctuates in this manner, as it is remarkable that the daily variation exceeds the stochastic fluctuation by such a large margin. This oddly narrow confidence interval is possibly due to the algorithm's failure to account for the appropriate type of variability. In contrast, the emulation method is the proper Bayesian representation of uncertainty.

Comparison for Synthetic R_t

Following the setup of the exercise in Section 3.2.2 that generates a synthetic R_t from a random normal distribution, we estimated the confidence interval from a Monte Carlo method with samples emulated from a state-space model.

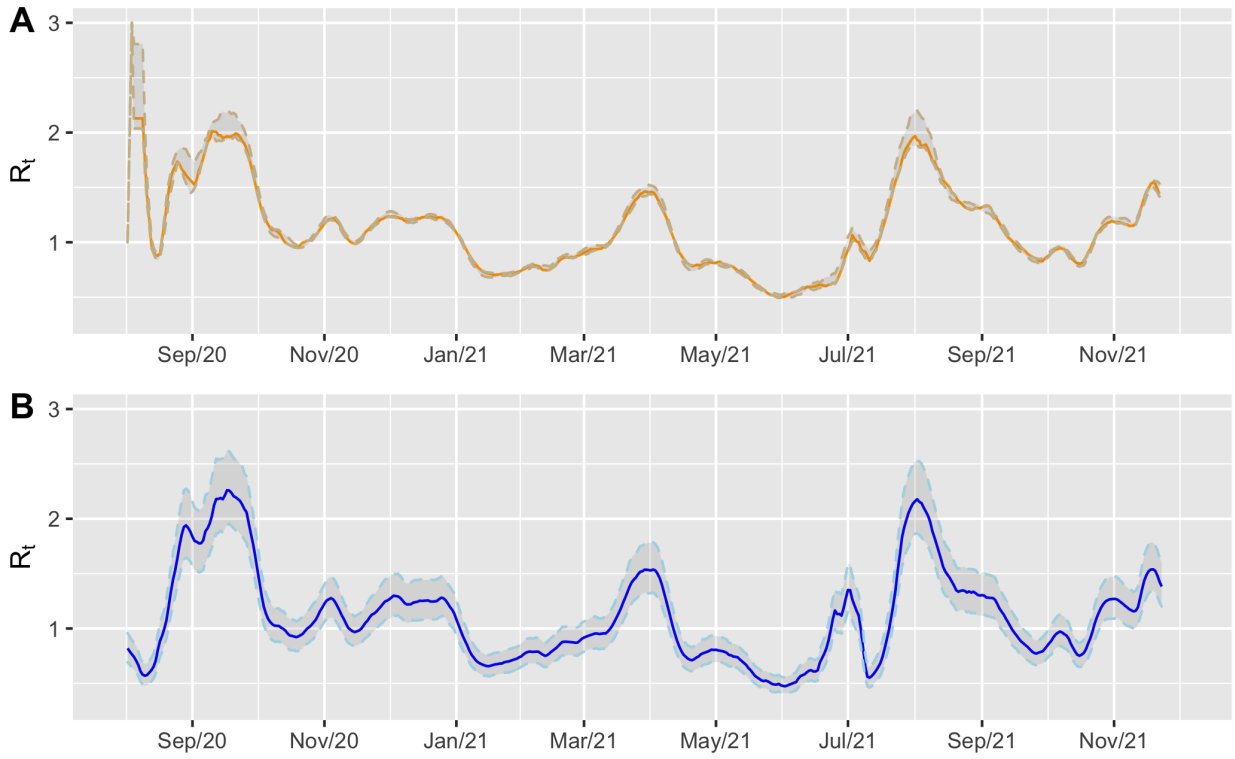

Figure 3.8: A. R_t and the estimated confidence interval using `EpiEstim` over the period from 1 April 2020 to 1 December 2021; B. R_t and its estimated confidence interval using the state-space model over the period from 1 April 2020 to 1 December 2021

Figure 3.9 compares R_t from the emulation and simulation-based methods with 2000 iterations for a seven-day window. It is obvious that the R_t from the simulation-based method developed by Cori et al. [7] has a much narrower confidence interval. This exercise illustrates that the cases can be reconstructed from a synthetic R_t, implying that the changes in R_t are natural fluctuations rather than reflections of the NPIs.

However, given that the confidence interval estimated by Cori et al. [7] is too small, changes in R_t might be misinterpreted as a reflection of the NPIs. In contrast, the confidence interval derived from the state-space model covers 1 most of the time, implying that the changes in R_t could be due to natural fluctuations and that the changes in such R_t do not reflect the impact of NPIs.

To reach a reasonable judgment about the effect of NPIs, one must carefully examine R_t and a corresponding confidence interval. An appropriate confidence interval can pro-

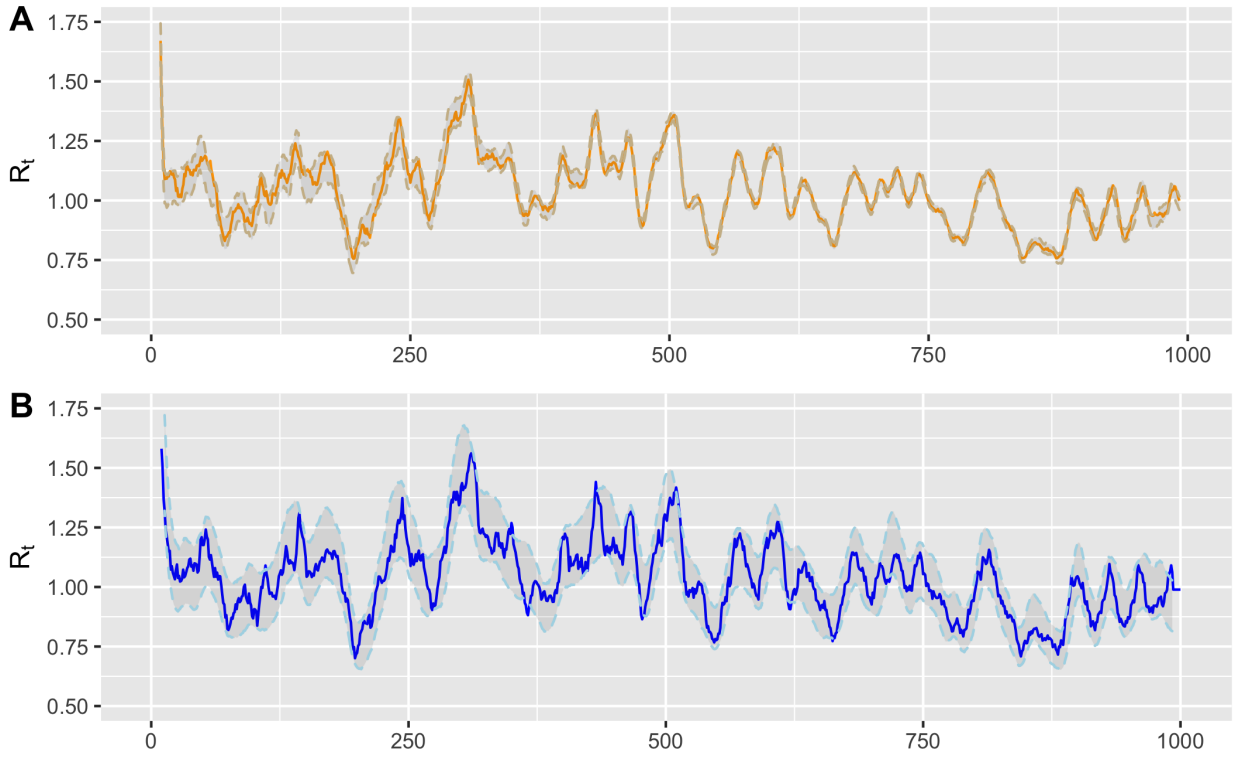

Figure 3.9: Comparison of R_t from the emulation and simulation-based methods with 2000 iterations for a seven-day window

vide an adequate representation of reality that accounts for methodological inaccuracies in the estimation process. The confidence interval produced by the state-space model reduces the bias due to the weakness of the algorithm and hence yields better results.

Chapter 4

The effect of NPIs

Evaluating the efficacy of NPIs in mitigating the spread of COVID-19 is critical to inform future preparedness response plans. A widely used metric that quantifies the impact of NPIs is the effective reproduction number, R_t. Chapter 3 discussed some weaknesses previously overlooked in the algorithm developed by Cori et al. [7] for estimating R_t.

In particular, the exercise in Section 3.2.2 demonstrated that it is crucial to examine the confidence interval when studying the effect of NPIs. Without a carefully calculated confidence interval, a hasty analysis could misinterpret the natural variation of R_t as the impact of NPIs. This thesis adopts the confidence interval from a state-space model, which was established in Section 3.3.

One NPI that may be regarded as too restrictive is a curfew, such as the one which was imposed by the Government of Québec from 9 January to 17 May 2021. Before the curfew, several other NPIs were implemented; thus, it remains uncertain if the change in R_t was caused by the curfew. This thesis proposes a control of variable strategy, in which the variable of interest is varied and other potential variables are controlled (held constant). Other potential variables that may influence the development of the disease include demographics, weather and variants.

Because Ontario never implemented any curfew and has demographics, weather and variants comparable to Québec, it is beneficial to draw a comparison for the number of

cases in Québec and Ontario over the same period that covers the implementation of the curfew, viz. September 2020 to July 2021. Therefore, the majority of the figures in this section cover data from 1 September 2020 to 1 July 2021, with a few exceptions focusing on 1 December 2020 to 1 June 2021.

4.1 Comparison With Ontario

Figure 4.1 shows the reported cases with a 95% confidence interval for Québec and Ontario; the confidence interval was estimated using 2000 samples emulated by the state-space model. A separate plot of the same scale is available in Section A.2 in the Appendix. Both curves have two peaks, reflecting the two waves of the disease during the period from 1 September 2020 to 1 July 2021. The first wave was roughly over the period from 15 October 2020 to 5 January 2021 from the start to peak; the second wave was roughly over the period from 1 March 2021 to 15 April 2021 from the start to peak.

The cases curve of Ontario has a much higher peak for the second wave. An obvious cause for the higher peak for Ontario is the difference in the total population, namely 14,789,778 for Ontario and 8,604,500 for Québec. The cases per 100,000 people were constructed based on the number of cases multiplied by 100,000 and divided by the population in each province, respectively.

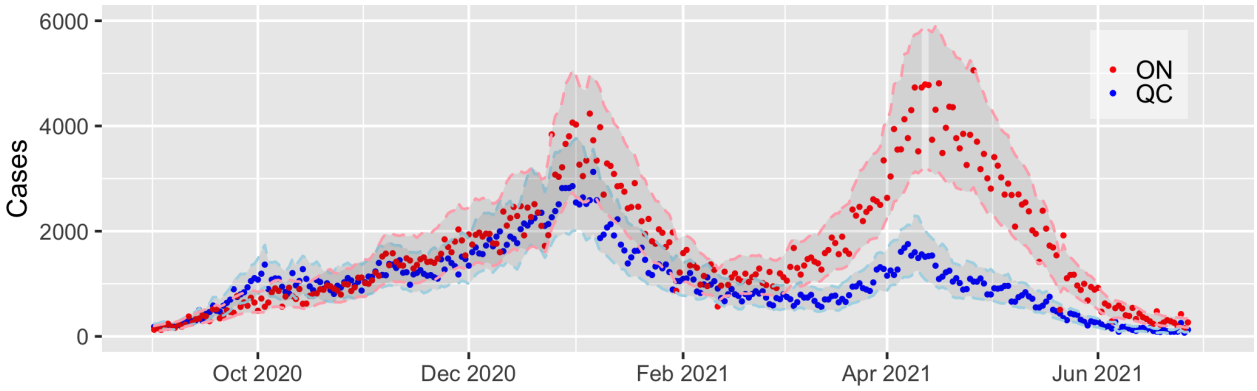

Figure 4.1: Reported cases and its estimated confidence interval over the period from 1 September 2020 to 1 July 2021 in Québec and Ontario

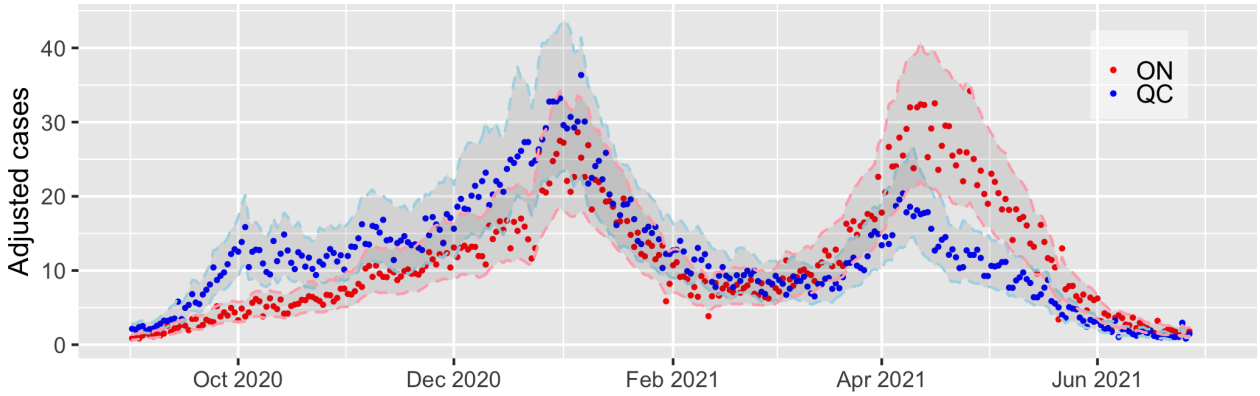

Figure 4.2: Cases per 100,000 people in Québec and Ontario over the period from 1 September 2020 to 1 July 2021

As shown in Figure 4.2, the difference in the peak for the second wave remains. Because the comparison is on cases per 100,000 people, this difference can no longer be justified by the difference in population. The cases per 100,000 people for Québec is slightly higher than that of Ontario before January and is approximately the same for the two provinces from 10 January to 1 March, demonstrating that the rate of transmission R_t is slightly higher in Québec from 10 January to 1 March and is approximately the same for the two provinces over the period from 1 January, 2020 to 1 March, 2021.

Why did the change of the peaks in the second wave differ for the two provinces? A possible explanation is that the two provinces implemented different policies to cope with the rise of the disease during the second wave.

Table 4.1 provides a list of NPIs implemented by the two provinces from 15 October 2020 to 5 January 2021.

Table 4.2 provides a list of NPIs implemented by the two provinces from 1 March to 15 April, 2021. Prior to the outbreak of the second wave, both provinces reopened elementary and secondary schools and non-essential businesses, with restrictions. Québec reopened elementary and secondary schools earlier, and reopened non-essential businesses slightly earlier. In particular, Québec reopened elementary schools on 11 January, and secondary schools on 18 January; Ontario reopened elementary and secondary schools on 8 February. Québec reopened non-essential businesses and restaurants on 8 February;

Table 4.1: Summary of NPIs for Québec and Ontario over the period from 15 October 2021 to 5 January 2021

	NPI	Date
QC	Closures of non-essential businesses in red zones extended	Prior
	Gatherings outside of household prohibited (certain regions)	Oct 22–Nov12
	Indoor/outdoor gatherings prohibited (certain regions)	Dec 7, Dec 14
	Elementary schools closed	Dec 17
	Non-essential businesses and restaurants closed	Dec 25
	Curfew between 8 p.m. and 5 a.m.	Jan 9
ON	Fitness closed; dine-in restricted to 10; Gatherings restricted to 5 indoor/25 outdoor. (certain regions).	Prior
	Dine-in prohibited Gatherings restricted to 5 indoor/25 outdoor.	Oct 19
	Indoor gatherings prohibited, outdoor gatherings limited to 10 people (certain regions).	Nov 7–Dec 14
	Non-essential businesses and restaurants closed (3 regions)	Dec 14
	Indoor gatherings prohibited, outdoor gatherings limited to 10 people.	Dec 26
	Non-essential businesses and restaurants closed	Dec 26
	Elementary and secondary schools moved to remote learning	Jan 4

Ontario slowly reopened non-essential businesses on 10 February, and indoor dining on 22 February. Moreover, Ontario relaxed the private gathering limit to 10 indoors/ 25 outdoors for 4 regions on 22 March. Québec relaxed the curfew to 9:30 p.m. on 17 March for certain regions.

In addition to the restrictions they already had, both provinces implemented swift and intense policies at the beginning of the second wave. Both provinces enforced restrictions on dining, retail, and gatherings. Of note, the curfew in Québec was in effect from January 2021, and further reinforced on 11 April 2021.

Table 4.2: Summary of NPIs for Québec and Ontario over the period from 1 March 2021 to 15 April 2021

	NPIs	Date
QC	Curfew in place from 8 p.m. to 5 a.m. (5 regions)	Prior
	Easing restrictions on place of worship (100 allowed); non-essential businesses reopened (4 regions)	March 8–26
	Primary and secondary schools closed. (3 regions)	April 1
	Curfew in effect between 8 p.m. and 5 a.m. (5 regions) Primary and secondary schools closed. (5 regions)	April 5
	Gyms and indoor public places for leisure and sports closed; maximum of 8 permitted for outdoor activities (red zones)	April 8
	Curfew in place from 8 p.m. to 5 a.m. (Montréal and Laval)	April 11
ON	Gatherings limited to 5 indoors/ 25 outdoors (certain regions).	Prior
	Gatherings limited to 5 indoors/ 10 outdoors (certain regions).	March 19–30
	Essential retail limited to 50% capacity, Non-essential retail limited to 25% capacity, Personal care services and in-person dining closed. Indoor events and social gatherings prohibited; Outdoor gatherings limited to 5; Indoor weddings and funerals limited to 15% capacity.	April 3
	Non-essential workplaces closed, Essential retail capacity reduced to 25%.	April 17
	Elementary and secondary schools moved to remote learning. Indoor and outdoor weddings and funerals limited to 10.	April 19

4.2 Comparison of Effective Reproduction Numbers

Figure 4.3 shows the estimated R_t with a 95% confidence interval over the period from October 2020 to July 2021 in Québec and Ontario with a seven-day window. The confidence interval was acquired using a state-space model with Kalman filter of 2000 iterations. On 10 April 2021, Québec had an R_t of 1.3802, with a 95% confidence interval $(1.2021, 1.5896)$. Ontario had an R_t of 1.8423 with a 95% confidence interval $(1.2962, 2.5737)$. Québec had a much lower R_t for the second peak. The comparisons of R_t for the two provinces for window sizes 1, 5, 7, and 14 of the same scale are available in Section A.4 in the Appendix.

As discussed in Section 3.2.2, it is essential to compare the R_t of the two provinces when their confidence intervals are mutually exclusive, as this indicates a significant dif-

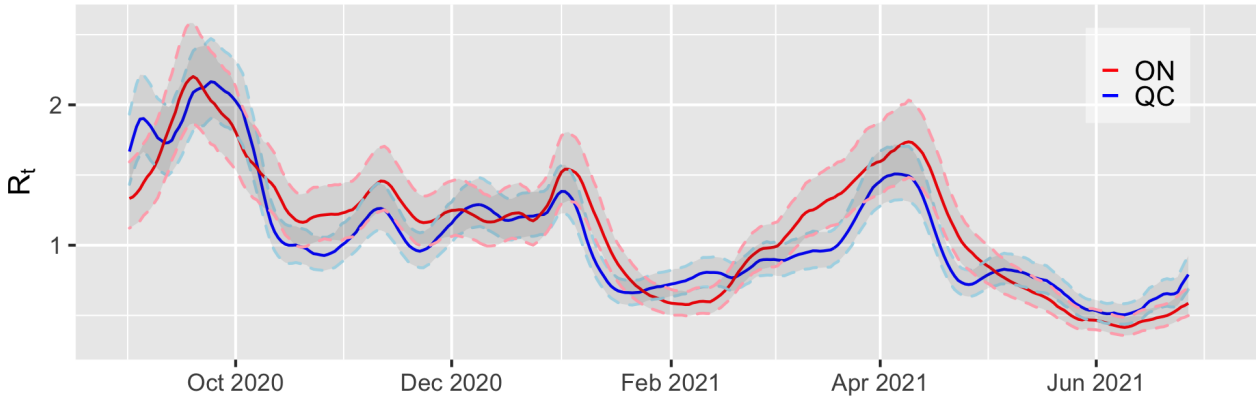

Figure 4.3: The estimated R_t with a 95% confidence interval in Québec and Ontario over the period from 1 September 2020 to 1 July 2021

ference in their transmission rates. There are three occasions on which the confidence intervals for the two provinces do not overlap: 8 February, 15 March, and 21 April.

Figure 4.4 shows the comparison of R_t for the two provinces with critical NPIs noted over the period from 1 December 2020 to 1 June 2021. The confidence interval for R_t

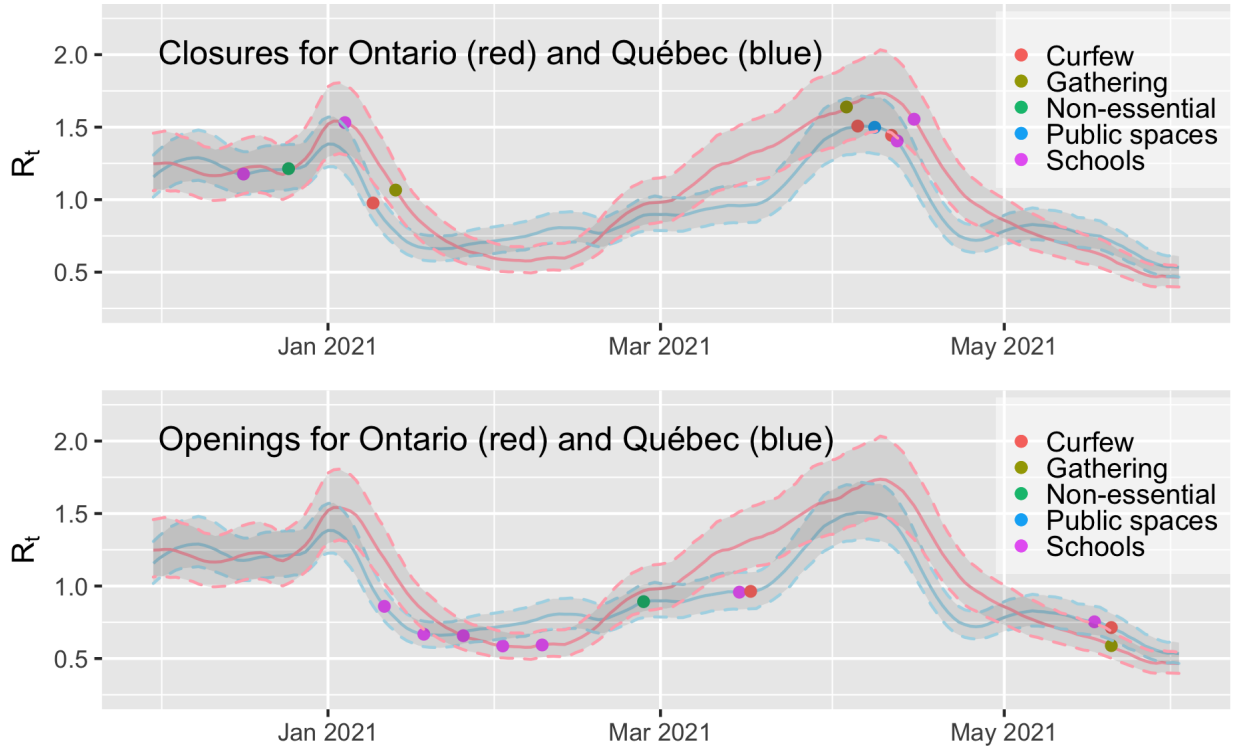

Figure 4.4: Comparison of R_t for the two provinces with critical NPIs noted over the period from 1 December 2020 to 1 June 2021

is calculated using 2000 samples emulated by the state-space model with a seven-day window. Section A.5 in the Appendix contains plots of the same scale over a longer time period and for the two provinces separately.

It is important to note that the confidence intervals for mid-February and mid-March are mutually exclusive; for 8 February, the upper bound for Ontario is lower than the lower bound for Québec. Because there is no overlap between the confidence intervals, we can draw conclusions without being influenced by the natural fluctuations of R_t. Considering the mutual exclusivity of confidence intervals for R_t, one can conclude with 95% certainty that the R_t for Ontario is significantly lower on 8 February and the R_t for Québec is significantly lower in mid-March.

Figure 4.5 shows the corresponding interventions on the plot for enhanced readability.

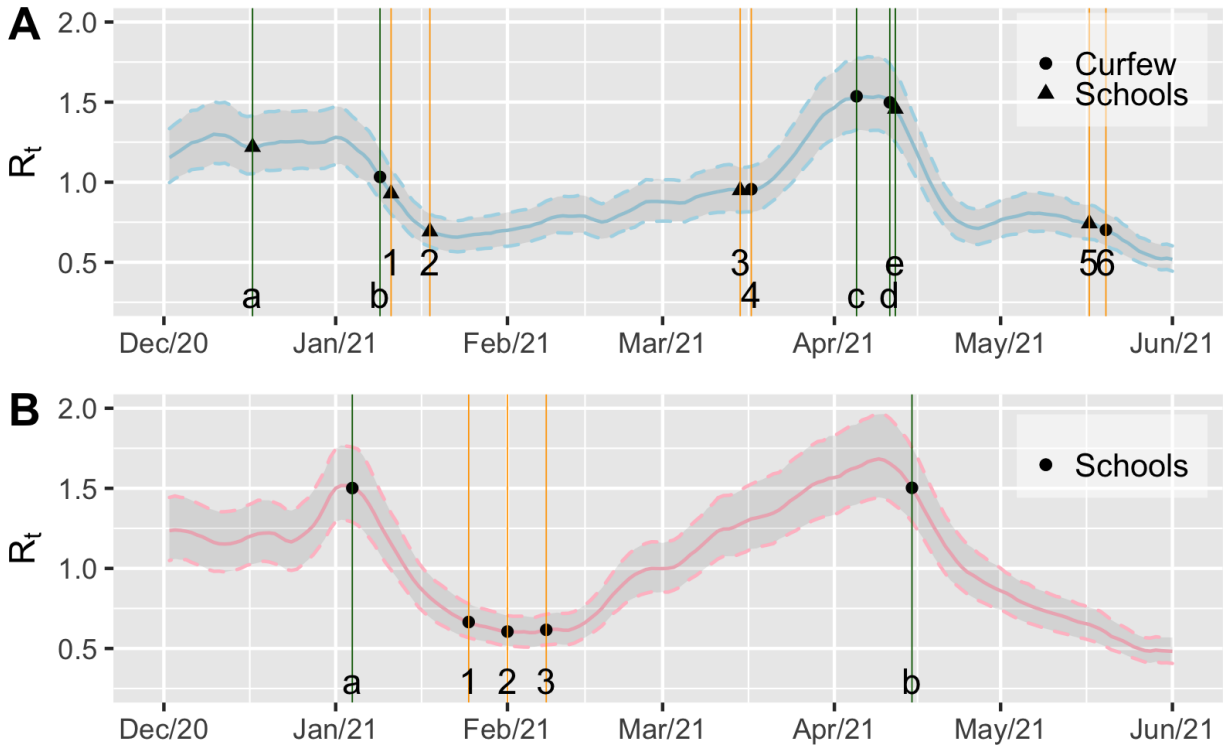

Figure 4.5: Comparison of R_t for the two provinces with selected NPIs noted over the period from 1 December 2020 to 1 June 2021

In panel A of Figure 4.5, letters are used to show the implementation of NPIs, viz.

a. Elementary schools closed on 17 December.

b. Curfew between 8 p.m. and 5 a.m. on 9 January.

c. Curfew in effect between 8 p.m. and 5 a.m. (5 regions) on 5 April.

d. Curfew in place from 8 p.m. to 5 a.m. (Montréal and Laval) on 11 April.

e. Students in Secondary 3, 4, and 5 will attend school in person every other day in combination with online learning (red zones).

Numerals are used to show the relaxation of NPIs, viz.

1. Elementary schools opened with masks mandated on 11 January.

2. Secondary schools opened with masks mandated on 18 January.

3. For regions in orange zones, extracurricular activities as well as school outings were permitted in stable class groups on 15 March.

4. For regions in red zones, the start of curfew moved to 9:30 p.m. on 17 March.

5. High school students resumed in-person learning; secondary 3, 4 and 5 students continued with a blended approach (Chaudière-Appalaches) on 17 May.

6. Curfew lifted in Côte-Nord on 21 May.

In panel B of Figure 4.5, the labels are used to indicate that:

a. Public and private elementary and secondary school students moved to teacher-led remote learning (7 public health regions) on 4 January;

b. Elementary and secondary schools moved to remote learning on 19 April;

1. Elementary and secondary schools resumed in-person learning with masks mandated for grades 1 to 3 (7 regions) on 25 January.

2. Elementary and secondary schools resumed in-person learning (4 additional public health units) on 1 February.

3. Elementary and secondary schools resumed in-person learning (13 additional public health units) on 9 February.

In both waves, the restrictions in Québec were less rigorous, except for the curfew. Québec had a moderately higher number of infections per 100,000 people at the start of the first wave, and Ontario had a slightly higher number of infections per 100,000 people at the start of the second wave.

For the first wave, the two provinces slowed R_t in two different ways: Ontario closed schools and Québec implemented curfews. Because for 20 January 2021, the upper bound for R_t for Québec is lower than the lower bound for R_t for Ontario, it may be concluded with 95% confidence that Québec was more effective in reducing R_t in the first wave.

Québec reopened elementary schools on 11 January and secondary schools on 18 January. Because Québec reopened schools earlier, there is a considerable gap in R_t for the two provinces around mid-February. The amount of increase of R_t for Québec was approximately 0.2 from mid-January to mid-February. In contrast, when Ontario opened schools on 8 February, R_t went up rapidly. The amount of increase of R_t for Ontario was around 0.7 from mid-February to mid-March. The most apparent explanation for the rise in R_t for Ontario is the opening of in-person school attendance.

Around 20 March 2021, there was a notable acceleration in the rate of increase of Québec's R_t. On 16 March, the curfew was pushed back to 9:30 p.m. for red zones, resulting in an immediate increase in the rate of change for R_t. The curfew had an immediate effect in this scenario.

A similar observation is reflected in the number of infections per 100,000 people. Even when the infections per 100,000 people in Québec were higher before mid-February, when they both had schools opened on 8 February, the number of infections in Québec per 100,000 people did not rise as much as in Ontario during the second wave.

A plausible criticism is that because Québec had more people infected and acquired temporary immunity, R_t would not increase as quickly, and therefore it is unclear whether the deceleration of R_t is due to the temporary immunity or the effect of the curfew.

There is a counter-argument. From 1 October to 31 December 2020, Québec had a higher per capita rate, so the number of people who could be infected in Québec was fewer due to waning of immunity, yet the two provinces had comparable values of R_t. It shows that Québec was at a more serious stage before the implementation of the curfew on 9 January 2021. It reinforces the idea that a curfew is beneficial for such a situation.

We were able to investigate two waves, with the second wave of in-person school attendance controlled for. Because both provinces allowed in-person school attendance throughout the second wave, we can give more weight to the contribution of the curfew. We can conclude that while schools are open, a curfew slows down the change in transmission rate.

To summarize, we found that: (i) there was evidence for an association between two NPIs (school closure and curfew) and reduced R_t; and (ii) while schools were open, a curfew slowed down the change in transmission rate.

4.3 Comparison of Death Curves

Figure 4.6 compares the reported and adjusted deaths over the period from 1 October 2020 to 1 July 2021 in Québec and Ontario. Ontario had a significant lower mortality rate per 100,000 people during the first wave and a slightly higher mortality rate per 100,000 people for the second wave.

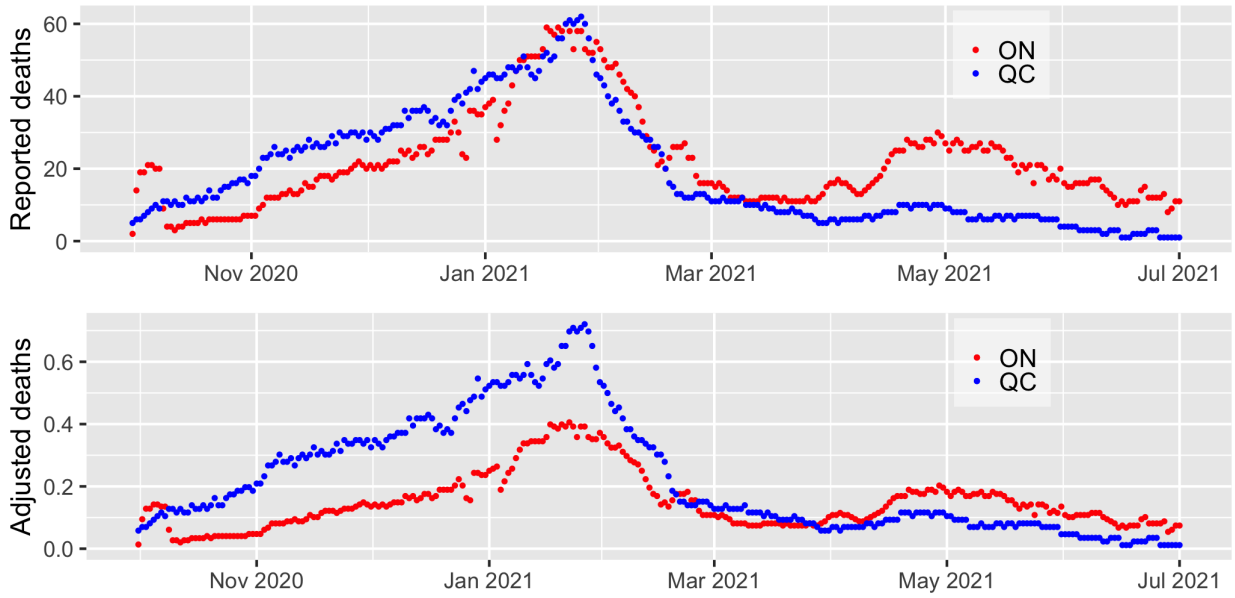

Figure 4.6: The reported and adjusted deaths in Québec and Ontario over the period from 1 October 2020 to 1 July 2021

Chapter 5

Change-Point Analysis

It is of interest to predict the case count in the absence of NPIs. A naive way to forecast the case count in the absence of curfews is to assume that the R_t stays the same after the day the curfew was imposed, then use Poisson regression to reconstruct the case count.

First, we retrieved the data of R_t and the number of cases with a 95% confidence interval from Section 3. Then, the `estimate_R` function was used to obtain the distribution of the serial interval w. A modified R_t was generated by replacing the R_t after the changing day with the R_t of the day. The changing day is the day on which the NPI we aim to investigate was imposed. We then inputted the distribution of serial interval w, the modified R_t and the cases curve I into the Poisson regression model to simulate case counts.

Similarly, the confidence interval was generated by inputting the distribution of the serial interval w, the modified lower or upper bound of the confidence interval for R_t and the cases curve I into the Poisson regression model to simulate case counts.

Figure 5.1 shows the forecasting of cases with constant R_t after 9 January and 11 April 2021 with 95% confidence interval, respectively. The curfew was first implemented in Québec on 9 January 2021 between 8 p.m. and 5 a.m.; it was later relaxed to 9:30 p.m. on 17 March. On 5 April, the curfew was extended to 8 p.m. in five regions; on 11 April, it was extended to Montréal and Laval.

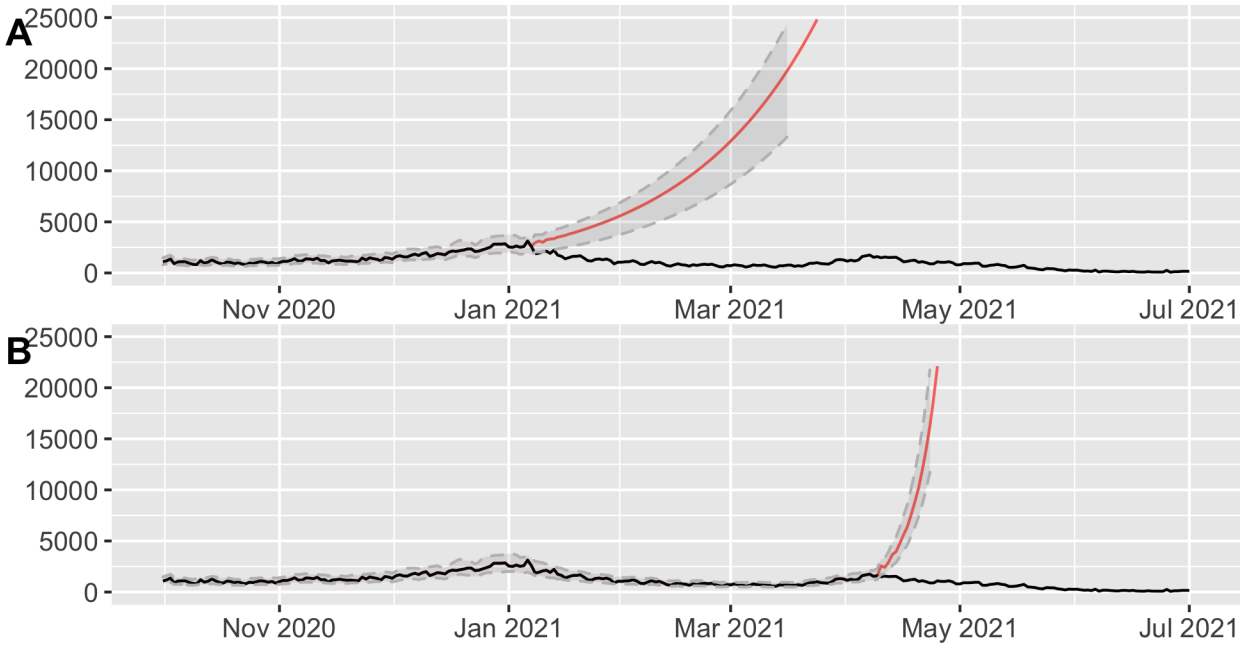

Figure 5.1: A. Simulated cases in the event that no curfew had been imposed on 9 January 2021 in Québec; B. Simulated cases in the event that no curfew had been reinforced on 11 April 2021 in Québec

If no curfew had been implemented on 9 January 2021, the number of cases on 31 May 2021 would be 171,693 and the corresponding 95% confidence interval would be (115,580; 211,579). That is, 20% of the population would be infected in around four months in the absence of curfews or equivalent NPIs.

If the curfew had not been reinforced on 11 April 2021, the number of cases on 31 May 2021 would be 5,603,516 and the corresponding 95% confidence interval would be (4,041,082; 7,498,861). That is, 70% of the population would be infected in less than two months in the absence of curfews or equivalent NPIs. The confidence interval in this scenario is much narrower than in the first, presumably because the confidence interval previous to the change date is narrower.

Although the model produces an artificial forecast, it is not a genuine projection. Even if there had been no curfew, the government or the people may have taken alternative measures if the pandemic was becoming too severe; for example, masses of people might then voluntarily choose to avoid crowded areas.

Chapter 6

Conclusion and Discussion

The main contributions of this thesis are to: (i) verify and improve the methodology of finding R_t; (ii) present a confidence interval for R_t; (iii) discuss the effectiveness of certain NPIs in Québec and Ontario; and iv) provide simple forecasts for the future incidence of COVID-19 in the absence of certain NPIs in Québec, Canada.

The impact of NPIs was measured by the effective reproduction number, R_t. We first introduced a widely used method for estimating R_t, the `EpiEstim` algorithm developed by Cori et al. [7]; it requires the number of cases and the distribution of serial intervals. Section 3.1.3 critically reviewed the `EpiEstim` method and showed that a feature of the estimation is that it reconstructs a somewhat wiggly R_t curves from a flat one. This seemingly innocuous inaccuracy in the estimation process may lead to false conclusions.

An appropriate confidence interval can provide an adequate representation of reality while accounting for methodological inaccuracies in the estimation process. Section 3.2.1 highlighted the issues with the algorithm of Cori et al. [7] in obtaining a meaningful confidence interval. The exercise in Section 3.2.2 demonstrated a serious ramification of failing to have a valid representation of uncertainty, namely that it can then become impossible to detect the nature of changes in R_t, possibly resulting in biased conclusions.

Section 3.3 devised a Monte Carlo approach for estimating R_t and a corresponding confidence interval. We examined two methods for generating samples, namely the

forward-simulation method, and state-space modelling. We discussed the advantages of obtaining the confidence interval generated using the Monte Carlo method with samples emulated by the state-space model.

We found that (i) there is evidence for an association between two NPIs (school closure and curfew) and reduced R_t; and (ii) curfew slows down the change in transmission rate when the controlled variable (school closure) is held constant. Some studies have reached conclusions consistent with ours. Liu et al. [15] found strong evidence for an association between two NPIs (school closure and internal movement restrictions) and reduced R_t. Yang et al. [21] demonstrated that implementation of control measures (large-scale quarantine and strict controls on travel) on 23 January 2020 in China was indispensable in limiting the eventual extent of the COVID-19 epidemic.

Nevertheless, some limitations should be mentioned. Many factors may result in inaccuracy in data collection and consequently inaccuracy in estimating R_t. First, COVID-19 testing and screening efforts or eligibility criteria vary by period. Changes in screening efforts influence the number of reported cases, which can cause an artificial change in R_t if the model perceives the change in case counts as a change in transmission rate.

A second limitation is the amount of available data. Because it is a relatively recent disease, data for Canada were only available as of March 2020. In comparison, data for similar epidemic diseases, such as measles and influenza, have been accessible for more than 50 years. Furthermore, the transmission rate of each variant of the disease varies. Because the Omicron variant is much more contagious, the Government of Québec instituted self-testing, which resulted in a substantially lower reporting rate. As a result, the data for this study are limited to the period from March 2020 to December 2021.

The third limitation is that we did not account for immunity in our analysis. During the first wave, there were no vaccines, but vaccination was initiated during the second wave. We assumed that the vaccination rates for Québec and Ontario were comparable due to similar demographics and vaccine availability.

One way to circumvent the inaccuracy of R_t estimation caused by the lack of available data is through international comparisons because the transmission rate remains constant for many countries for the same variant of COVID-19.

Bibliography

[1] BERRY, I., O'NEILL, M., STURROCK, S. L., WRIGHT, J. E., ACHARYA, K., BRANKSTON, G., HARISH, V., KORNAS, K., MAANI, N., NAGANATHAN, T., OBRESS, L., ROSSI, T., SIMMONS, A. E., VAN CAMP, M., XIE, X., TUITE, A. R., GREER, A. L., FISMAN, D. N., AND SOUCY, J.-P. R. A sub-national real-time epidemiological and vaccination database for the COVID-19 pandemic in Canada. *Scientific Data 8*, 1 (July 2021), 173.

[2] BJØRNSTAD, O. N., SHEA, K., KRZYWINSKI, M., AND ALTMAN, N. The SEIRS model for infectious disease dynamics. *Nature Methods 17*, 6 (June 2020), 557–558.

[3] BRAUNER, J. M., MINDERMANN, S., SHARMA, M., JOHNSTON, D., SALVATIER, J., GAVENČIAK, T., STEPHENSON, A. B., LEECH, G., ALTMAN, G., MIKULIK, V., NORMAN, A. J., MONRAD, J. T., BESIROGLU, T., GE, H., HARTWICK, M. A., TEH, Y. W., CHINDELEVITCH, L., GAL, Y., AND KULVEIT, J. Inferring the effectiveness of government interventions against COVID-19. *Science 371*, 6531 (2021), eabd9338.

[4] CANADIAN INSTITUTE FOR HEALTH INFORMATION. COVID-19 Intervention Scan–Data Tables. `https://www.cihi.ca/en/covid-19-intervention-timeline-in-canada`, 2021. Last accessed on 22 July 2022.

[5] CAO, Z., ZHANG, Q., LU, X., PFEIFFER, D., JIA, Z., SONG, H., AND ZENG, D. D. Estimating the effective reproduction number of the 2019-nCoV in China. *medRxiv* (2020).

[6] CONSTANTINESCO, A., ISRAEL-JOST, V., AND CHOQUET, P. Spectral analysis of the daily evolution of deaths due to COVID-19 in France and in the world shows a weekend effect: Myth or reality? *medRxiv* (January 2020), 2020.06.23.20135442.

[7] CORI, A., FERGUSON, N. M., FRASER, C., AND CAUCHEMEZ, S. A new framework and software to estimate time-varying reproduction numbers during epidemics. *American Journal of Epidemiology 178*, 9 (September 2013), 1505–1512.

[8] FERGUSON, N., LAYDON, D., NEDJATI-GILANI, G., IMAI, N., AINSLIE, K., BAGUELIN, M., BHATIA, S., BOONYASIRI, A., CUCUNUBÁ, Z. M., CUOMO-DANNENBURG, G., DIGHE, A., DORIGATTI, I., FU, H., GAYTHORPE, K., GREEN, W., HAMLET, A., HINSLEY, W., OKELL, L., VAN ELSLAND, S., AND GHANI, A. *Report 9: Impact of Non-Pharmaceutical Interventions (NPIs) to Reduce COVID-19 Mortality and Healthcare Demand*. MRC Centre for Global Infectious Disease Analysis, Imperial College, London, UK, March 2020.

[9] FLAXMAN, S., MISHRA, S., GANDY, A., UNWIN, H. J. T., MELLAN, T. A., COUPLAND, H., WHITTAKER, C., ZHU, H., BERAH, T., EATON, J. W., MONOD, M., PEREZ-GUZMAN, P. N., SCHMIT, N., CILLONI, L., AINSLIE, K. E. C., BAGUELIN, M., BOONYASIRI, A., BOYD, O., CATTARINO, L., COOPER, L. V., CUCUNUBÁ, Z., CUOMO-DANNENBURG, G., DIGHE, A., DJAAFARA, B., DORIGATTI, I., VAN ELSLAND, S. L., FITZJOHN, R. G., GAYTHORPE, K. A. M., GEIDELBERG, L., GRASSLY, N. C., GREEN, W. D., HALLETT, T., HAMLET, A., HINSLEY, W., JEFFREY, B., KNOCK, E., LAYDON, D. J., NEDJATI-GILANI, G., NOUVELLET, P., PARAG, K. V., SIVERONI, I., THOMPSON, H. A., VERITY, R., VOLZ, E., WALTERS, C. E., WANG, H., WANG, Y., WATSON, O. J., WINSKILL, P., XI, X., WALKER, P. G. T., GHANI, A. C., DONNELLY, C. A., RILEY, S., VOLLMER, M. A. C., FERGUSON, N. M., OKELL, L. C., BHATT, S., AND IMPERIAL COLLEGE COVID-19 RESPONSE TEAM. Estimating the effects of non-pharmaceutical interventions on COVID-19 in Europe. *Nature 584*, 7820 (August 2020), 257–261.

[10] GOLDSTEIN, E., DUSHOFF, J., MA, J., PLOTKIN, J. B., EARN, D. J. D., AND LIPSITCH, M. Reconstructing influenza incidence by deconvolution of daily mortality time series. *Proceedings of the National Academy of Sciences 106*, 51 (2009), 21825–21829.

[11] GOSTIC, K. M., MCGOUGH, L., BASKERVILLE, E. B., ABBOTT, S., JOSHI, K., TEDIJANTO, C., KAHN, R., NIEHUS, R., HAY, J. A., DE SALAZAR, P. M., HELLEWELL, J., MEAKIN, S., MUNDAY, J. D., BOSSE, N. I., SHERRAT, K., THOMPSON, R. N., WHITE, L. F., HUISMAN, J. S., SCIRE, J., BONHOEFFER, S., STADLER, T., WALLINGA, J., FUNK, S., LIPSITCH, M., AND COBEY, S. Practical considerations for measuring the effective reproductive number, R_t. *PLoS Computational Biology 16*, 12 (December 2020), e1008409.

[12] GU, Y. Estimating true infections revisited: A simple nowcasting model to estimate prevalent cases in the US. `https://covid19-projections.com/estimating-true-infections-revisited/`, 2020. Last accessed on 22 July 2022.

[13] HAUG, N., GEYRHOFER, L., LONDEI, A., DERVIC, E., DESVARS-LARRIVE, A., LORETO, V., PINIOR, B., THURNER, S., AND KLIMEK, P. Ranking the effectiveness of worldwide COVID-19 government interventions. *Nature Human Behaviour 4*, 12 (December 2020), 1303–1312.

[14] LIPSITCH, M., COHEN, T., COOPER, B., ROBINS, J. M., MA, S., JAMES, L., GOPALAKRISHNA, G., CHEW, S. K., TAN, C. C., SAMORE, M. H., FISMAN, D., AND MURRAY, M. Transmission dynamics and control of severe acute respiratory syndrome. *Science 300*, 5627 (May 2003), 1966–1970.

[15] LIU, Y., MORGENSTERN, C., KELLY, J., LOWE, R., MUNDAY, J., VILLABONA-ARENAS, C. J., GIBBS, H., PEARSON, C. A. B., PREM, K., LECLERC, Q. J., MEAKIN, S. R., EDMUNDS, W. J., JARVIS, C. I., GIMMA, A., FUNK, S., QUAIFE, M., RUSSELL, T. W., EMORY, J. C., ABBOTT, S., HELLEWELL, J., TULLY, D. C., HOUBEN,

R. M. G. J., O'REILLY, K., GORE-LANGTON, G. R., KUCHARSKI, A. J., AUZENBERGS, M., QUILTY, B. J., JOMBART, T., ROSELLO, A., BRADY, O., ATKINS, K. E., VAN ZANDVOORT, K., RUDGE, J. W., ENDO, A., ABBAS, K., SUN, F. Y., PROCTER, S. R., CLIFFORD, S., FOSS, A. M., DAVIES, N. G., CHAN, Y.-W. D., DIAMOND, C., BARNARD, R. C., EGGO, R. M., DEOL, A. K., NIGHTINGALE, E. S., SIMONS, D., SHERRATT, K., MEDLEY, G., HUÉ, S., KNIGHT, G. M., FLASCHE, S., BOSSE, N. I., KLEPAC, P., JIT, M., AND CMMID COVID-19 WORKING GROUP. The impact of non-pharmaceutical interventions on SARS-CoV-2 transmission across 130 countries and territories. *BMC Medicine 19*, 1 (February 2021), 40.

[16] MAHEU-GIROUX, M. Taux de reproduction (R_t) des cas de SRAS-CoV-2 au Québec. `https://www.inspq.qc.ca/covid-19/donnees/rt`. Last accessed on 22 July 2022.

[17] NASH, J. C. On best practice optimization methods in R. *Journal of Statistical Software 60*, 2 (2014), 1–14.

[18] NOUVELLET, P., BHATIA, S., CORI, A., AINSLIE, K. E. C., BAGUELIN, M., BHATT, S., BOONYASIRI, A., BRAZEAU, N. F., CATTARINO, L., COOPER, L. V., COUPLAND, H., CUCUNUBA, Z. M., CUOMO-DANNENBURG, G., DIGHE, A., DJAAFARA, B. A., DORIGATTI, I., EALES, O. D., VAN ELSLAND, S. L., NASCIMENTO, F. F., FITZJOHN, R. G., GAYTHORPE, K. A. M., GEIDELBERG, L., GREEN, W. D., HAMLET, A., HAUCK, K., HINSLEY, W., IMAI, N., JEFFREY, B., KNOCK, E., LAYDON, D. J., LEES, J. A., MANGAL, T., MELLAN, T. A., NEDJATI-GILANI, G., PARAG, K. V., PONS-SALORT, M., RAGONNET-CRONIN, M., RILEY, S., UNWIN, H. J. T., VERITY, R., VOLLMER, M. A. C., VOLZ, E., WALKER, P. G. T., WALTERS, C. E., WANG, H., WATSON, O. J., WHITTAKER, C., WHITTLES, L. K., XI, X., FERGUSON, N. M., AND DONNELLY, C. A. Reduction in mobility and COVID-19 transmission. *Nature Communications 12*, 1 (March 2021), 1090.

[19] ONTARIO GOVERNMENT. Ontario population projections. https://www.ontario.ca/page/ontario-population-projections, 2020. Last accessed on 22 July 2022.

[20] WACKERLY, D. D., MENDENHALL, W., AND SCHEAFFER, R. L. *Mathematical Statistics with Applications-Cengage Learning*, 7th ed. Thomson Higher Education, Belmont, CA, 2008.

[21] YANG, Z., ZENG, Z., WANG, K., WONG, S.-S., LIANG, W., ZANIN, M., LIU, P., CAO, X., GAO, Z., MAI, Z., LIANG, J., LIU, X., LI, S., LI, Y., YE, F., GUAN, W., YANG, Y., LI, F., LUO, S., XIE, Y., LIU, B., WANG, Z., ZHANG, S., WANG, Y., ZHONG, N., AND HE, J. Modified SEIR and AI prediction of the epidemics trend of COVID-19 in China under public health interventions. *Journal of Thoracic Disease 12*, 3 (March 2020), 165–174.

Appendix A

Appendix

A.1 NPIs for Québec over the period from 1 April 2020 to 1 December 2021

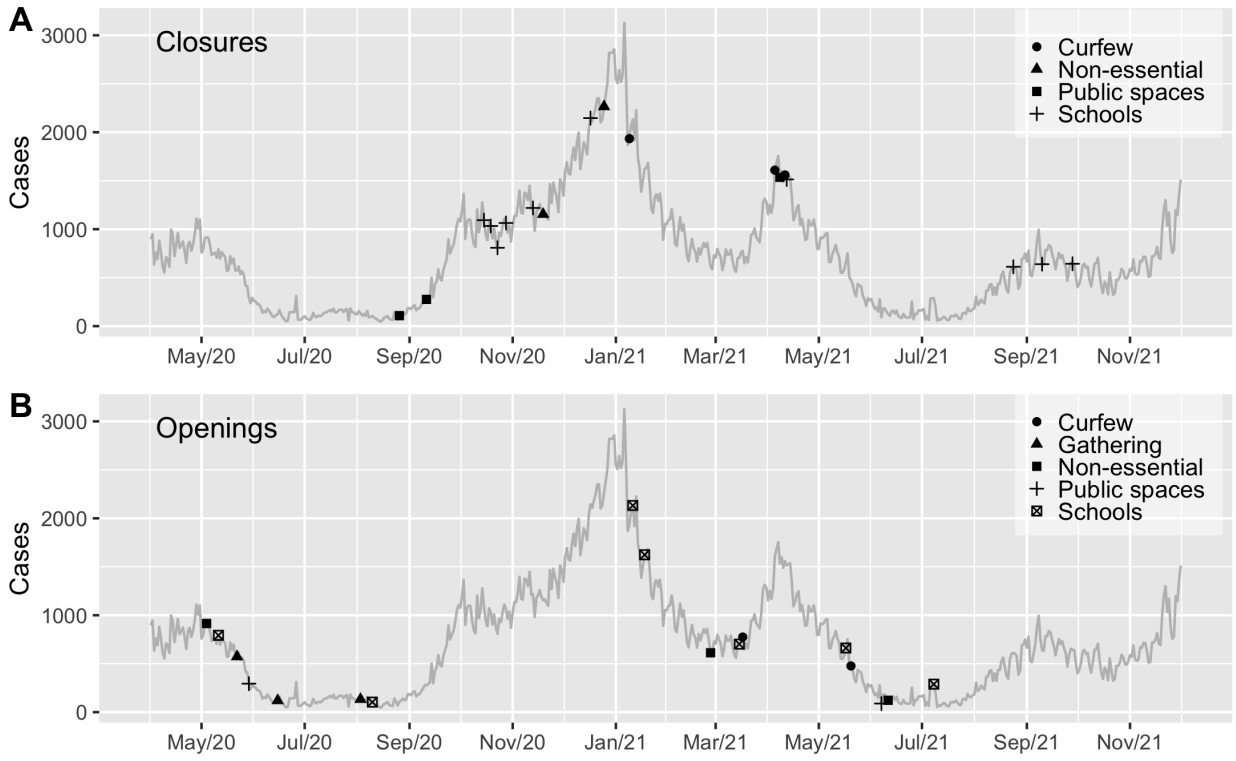

This plot is discussed in Section 2.5.2

A.2 Reported cases with confidence interval over the period from 1 October 2020 to 1 July 2021 in Québec and Ontario

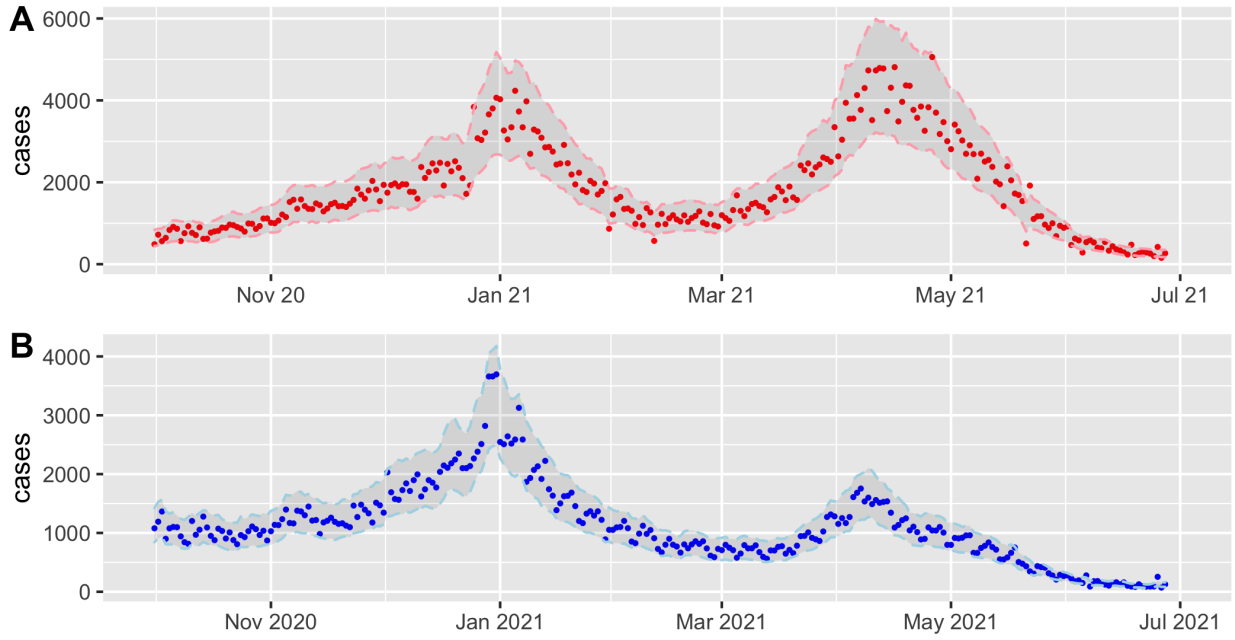

Panel A and Panel B of A.2 show the reported cases and the estimated confidence interval over the period from October 2020 to July 2021 in Québec and Ontario (in separate plots) with 2000 iterations respectively. This plot is discussed in Section 4.1

A.3 Effective reproduction number for window sizes 1, 5, 7, and 14 over the period from 1 December 2020 to 1 June 2021 for Québec and Ontario individually

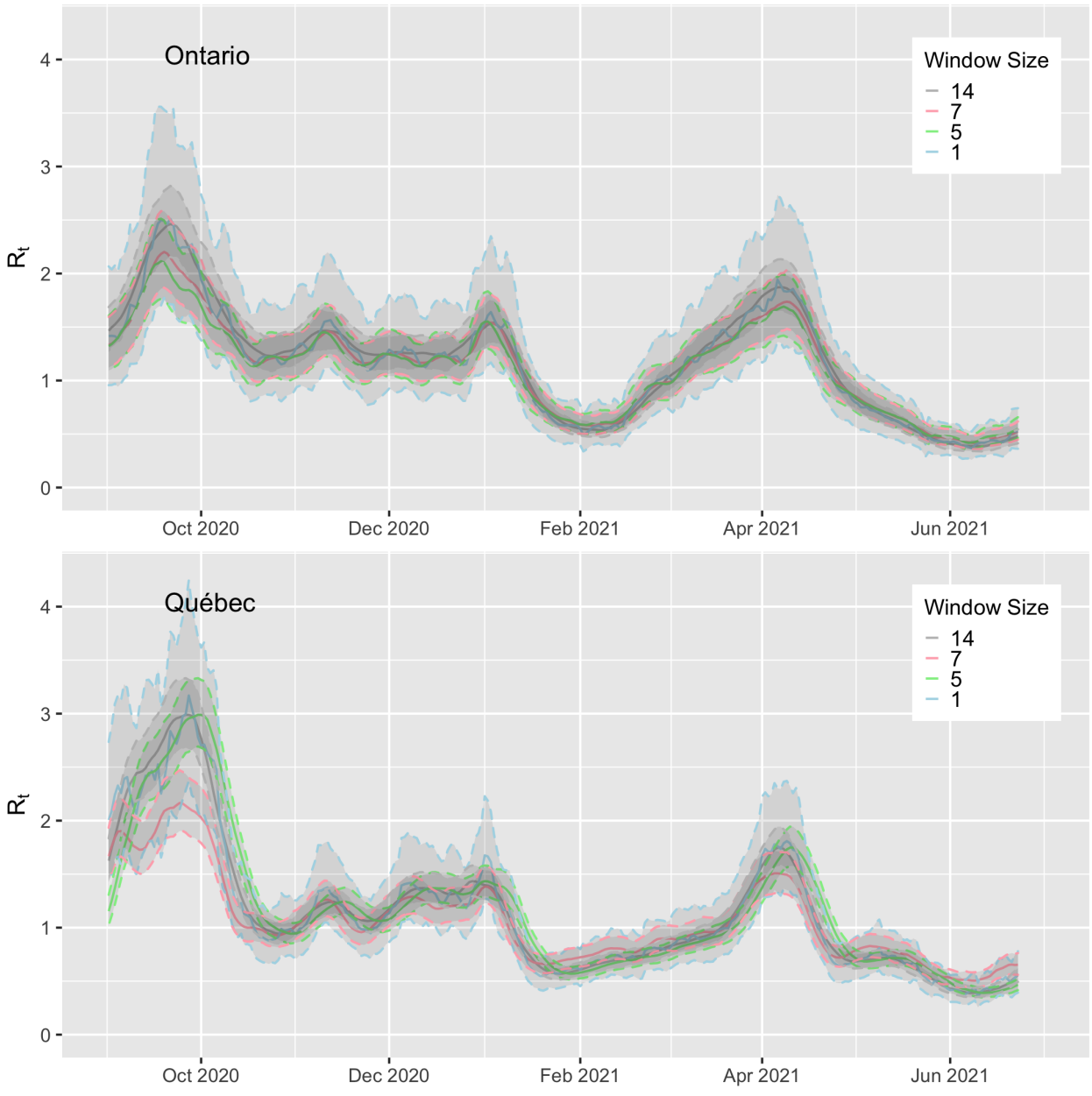

This plot is discussed in Section 4.2.

A.3.1 Effective reproduction number for window sizes 1, 5, 7, and 14 over the period from 1 December 2020 to 1 June 2021 for Québec and Ontario individually

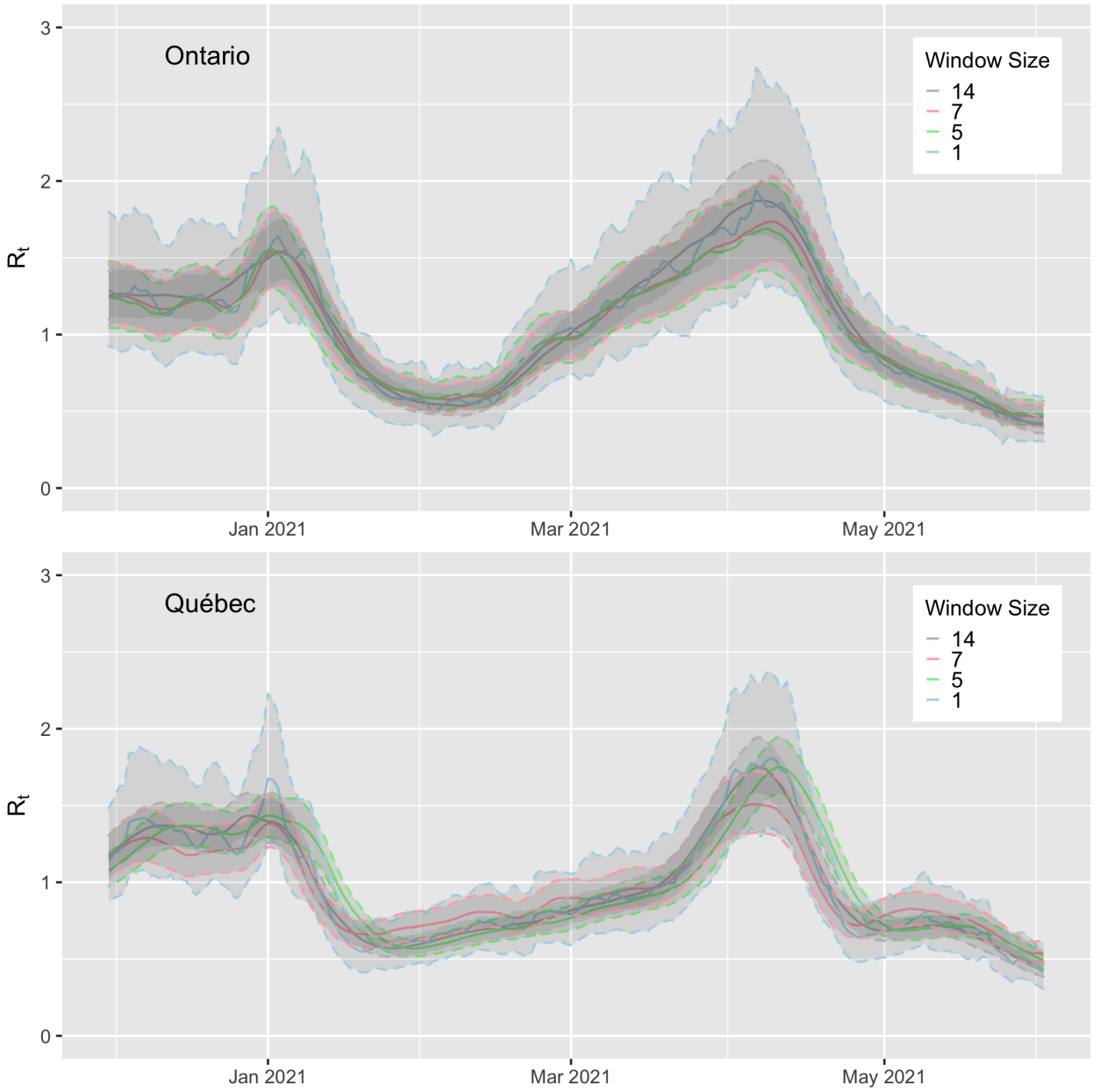

This plot is discussed in Section 4.2.

A.4 Comparison of effective reproduction numbers for window sizes 1, 5, 7, and 14 for Québec and Ontario over the period from 1 September 2020 to 1 July 2021

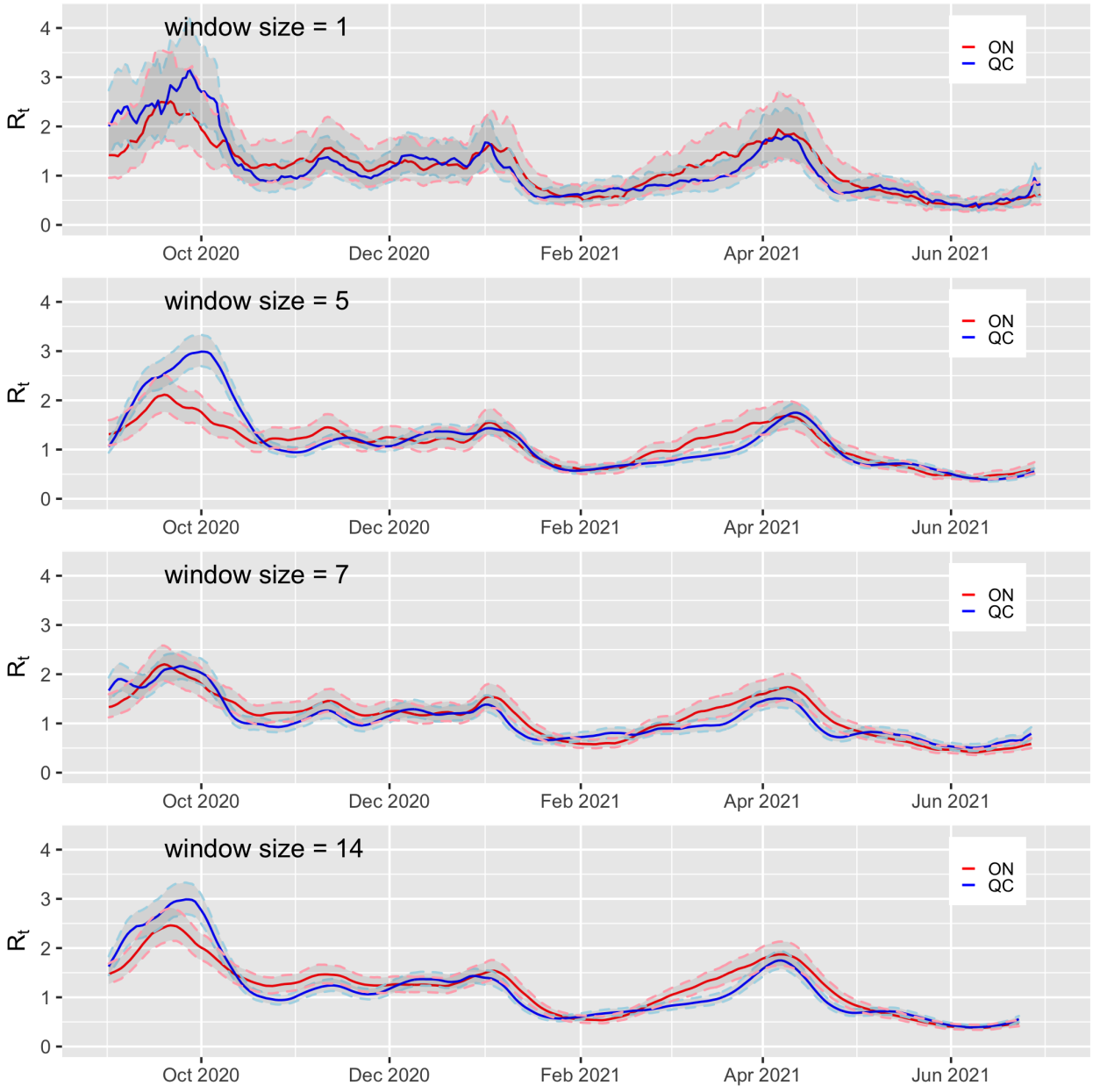

This plot is discussed in Section 4.2.

A.4.1 Comparison of effective reproduction numbers for window sizes 1, 5, 7, and 14 for Québec and Ontario over the period from 1 December 2020 to 1 June 2021

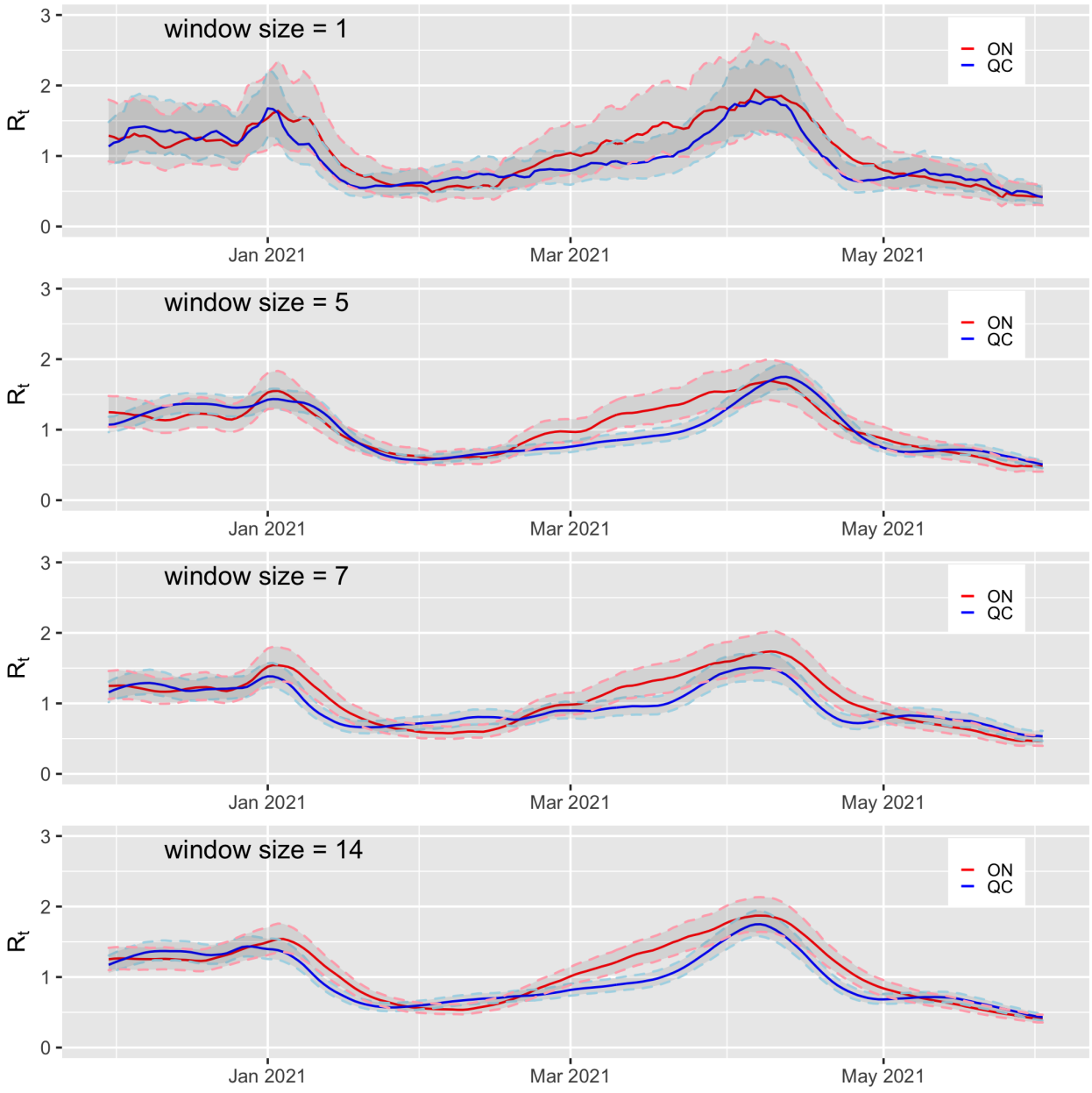

This plot is discussed in Section 4.2.

A.5 Effective reproduction number for Québec and Ontario over the period from 1 December 2020 to 1 June 2021

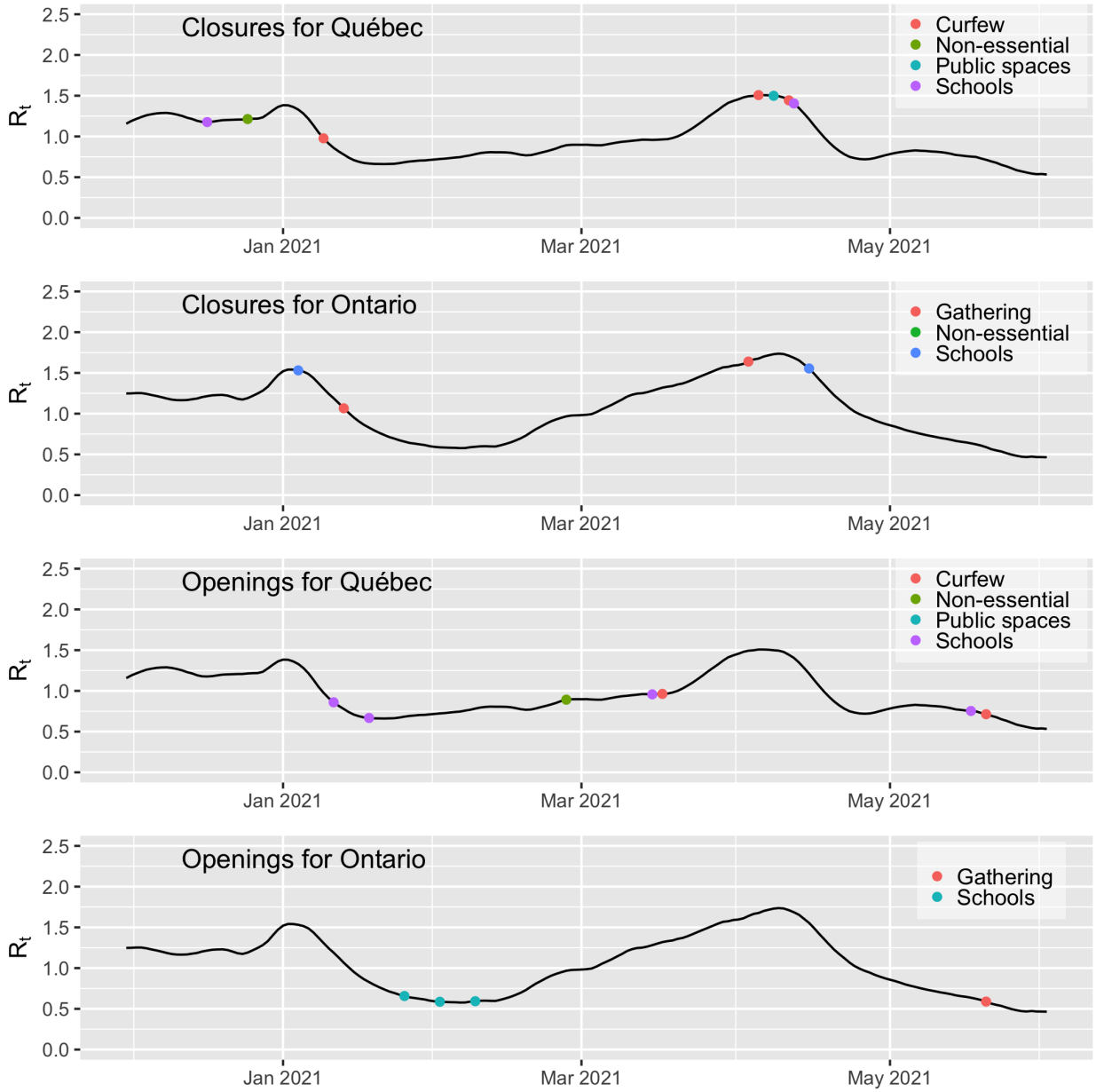

This plot is discussed in Section 4.2.

A.5.1 Effective reproduction number for Québec and Ontario with confidence interval over the period from 1 December 2020 to 1 June 2021

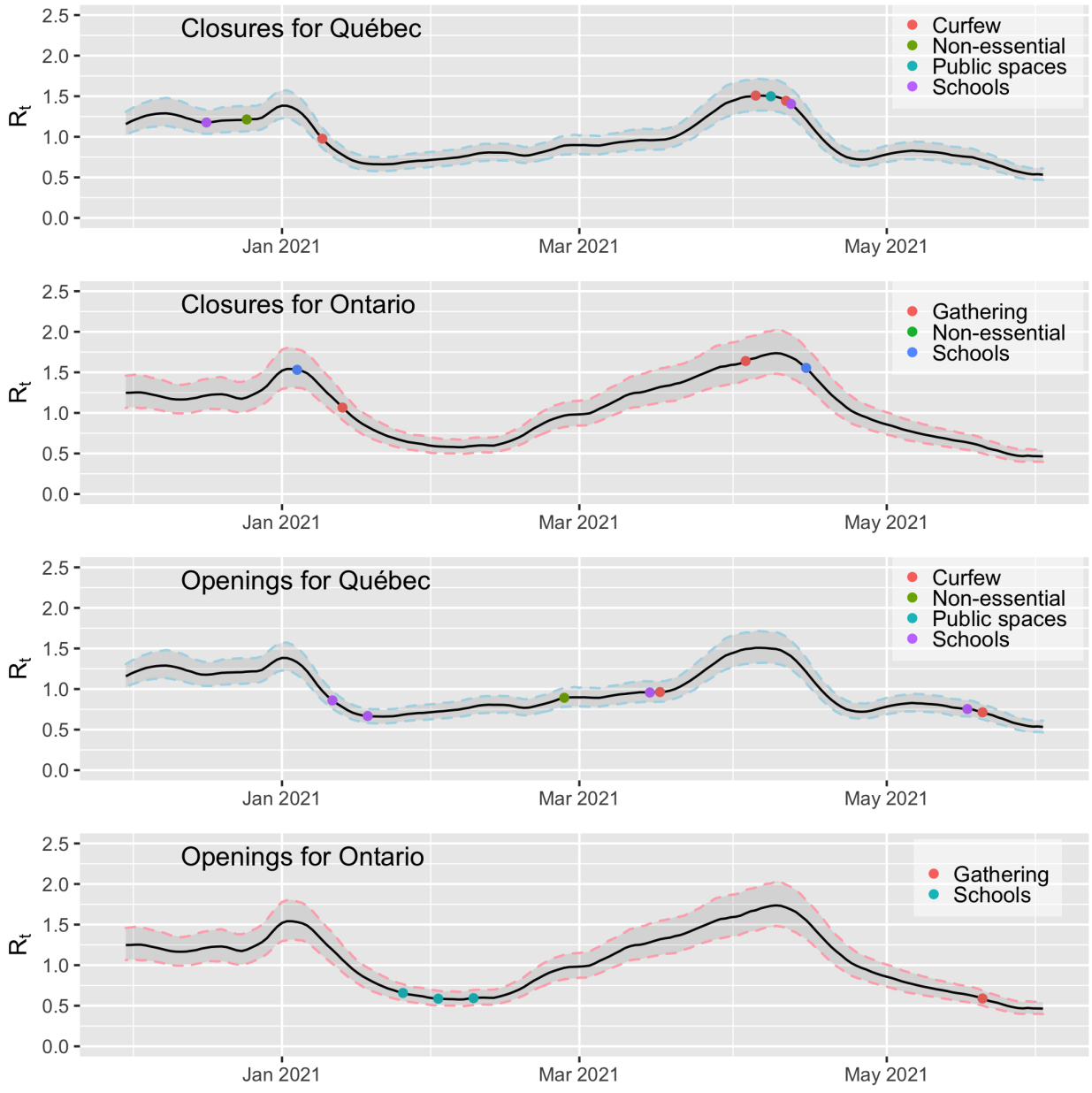

This plot is discussed in Section 4.2.